Earth-Science Reviews 248 (2024) 104631

Contents lists available at ScienceDirect

Earth-Science Reviews

journal homepage: www.elsevier.com/locate/earscirev

Physical geomorphometry for elementary land surface segmentation and digital geomorphological mapping

Jozef Minár [a,*], Lucian Drăguţ [b], Ian S. Evans [c], Richard Feciskanin [a], Michal Gallay [d], Marián Jenčo [a], Anton Popov [a]

[a] Department of Physical Geography and Geoinformatics, Faculty of Natural Sciences, Comenius University, Ilkovičova 6, Mlynská dolina B1, SK-842 15 Bratislava, Slovak Republic
[b] Department of Geography, West University of Timişoara, Bd. V. Parvan 4, 300223 Timişoara, Romania
[c] Geography Department, Durham University, Durham DH1 3LE, UK
[d] Institute of Geography, Faculty of Science, Pavol Jozef Šafárik University in Košice, Jesenná 5, 040 01 Košice, Slovakia

ARTICLE INFO

Dedicated to the memory of prof. Jozef Krcho (1934–2022), one of the founders of physically-based geomorphometry.

Keywords:
Geomorphometry
Landscape classification
Digital geomorphological mapping
Elementary forms
Curvatures
GEOBIA
Equilibrium
Energy

ABSTRACT

By interpretations related to energy, elementary land surface segmentation can be treated as a physical problem. Many pieces of such a view found in the literature can be combined into a synthetic comprehensive physical approach. The segmentation has to be preceded by defining the character and size of searched units to result from the segmentation. A high-resolution digital elevation model (DEM) is the key input for this task; it should be generalized to the resolution best expressing information about the searched units. Elementary land surface units can be characterized by various parts of potential gravitational energy associated with a set of basic geomorphometric variables. Elevation above sea level (z) represents Global Geomorphic Energy (*GGE*). Regional and Local Geomorphic Energy (*RGE* and *LGE*) are parts of *GGE*, represented respectively by relative elevation above the local base level (z_{rel}) and local relief (elevation differential in a moving window Δz). Derivation (change) of elevation defines the slope inclination (S), determining the local Potential Energy of Surface (*PES*) applicable to mass flow. Normal slope line (profile) curvature $(k_n)_s$ and normal contour (tangential) curvature $(k_n)_c$ express change in the *PES* value ($\Delta PES_{(k_n)_s}$, $\Delta PES_{(k_n)_c}$), responsible for acceleration/deceleration and convergence/divergence of flow. Mean curvature (k_{mean}) determines the Potential Energy of Surface applicable to Diffusion (*PESD*). Energetic interpretation of basic geomorphometric variables enables their direct comparison and systematic evaluation. Consequently, the homogeneity of basic geomorphometric variables defines a hierarchy of states of local geomorphic equilibria: static equilibrium, steady state, and non-steady state dynamic equilibrium. They are local attractors of landform development reflected in the geomorphometric tendency to symmetry (horizontality, various types of linearity, and curvature isotropy, together expressed by gravity concordance). Nonequilibrium and transitional states can be characterized by the PES excess (PES_e) determined by difference curvature (k_d), by gravity discordant change of the *PES* characterized by twisting curvature $(\tau_g)_c$, and by Integral Potential Energy of Surface Curvature (*IPESC*) expressed by Casorati curvature (k_C) (general curvedness). Excluding z_{rel} and Δz, all these energy-related geomorphometric variables are local point-based. Local area-based and regional variables such as Glock's Available Relief, Melton Ruggedness Number, Stream Power Index, Openness, Topographic Position Index, Topographic Wetness Index, and Index of Connectivity also have energetic interpretations although their definition is more complex. Therefore we suggest exclusive use of the local point-based variables in designs of elementary land surface segmentation. The segmentation should take notice of natural interconnections, the hierarchy of geomorphometric variables, elements of Local Geomorphic Energy, and (dis)equilibria states, so that elementary segments are clearly interpretable geomorphologically. This is exemplified by Geographic Object-Based Image Analysis (GEOBIA) segmentation of Sandberg, a territory on the boundary of the Carpathians and Vienna Basin with a complex geomorphic history and marked morphodynamics. Compared with expert-driven field geomorphological mapping, the automatic physically-based segmentation resulted in a more specific delineation and composition of landforms. Physical-geomorphometric characteristics of the elementary forms enabled the formulation of their system and subsequent improvement of

* Corresponding author.
E-mail address: jozef.minar@uniba.sk (J. Minár).

https://doi.org/10.1016/j.earscirev.2023.104631
Received 14 December 2022; Received in revised form 13 November 2023; Accepted 17 November 2023
Available online 26 November 2023

the expert-based qualitative genetic analysis, with interpretation leading to a deeper understanding of the development and recent dynamics of the landscape.

Abbreviations, symbols, and physical dimensions

Acceleration due to gravity g [m.s^{-2}]
Cartesian coordinate system (in plan) x, y [m]
Casorati curvature (general curvedness) k_C [m^{-1}]
Change of normal contour (tangential) curvature in direction of slope line $(k_n)_{cs}$ [m^{-2}]
Change of normal contour (tangential) curvature in direction of contour line $(k_n)_{cc}$ [m^{-2}]
Change of normal slope line (profile) curvature in direction of slope line $(k_n)_{ss}$ [m^{-2}]
Contour direction distance cd [m] (used as unit distance, $cd = 1$ m)
Contour geodesic torsion (twisting curvature) $(\tau_g)_c$ [rad.m^{-1}]
Density of material ρ [kg.m^{-3}]
Denudation Δh [m]
Difference curvature k_d [m^{-1}]
Diffusion coefficient κ [m^2.s^{-1}]
Direction of (tangent to) contour line c
Direction of (tangent to) slope line s
Distance to nearest stream ds [m]
Downslope distance d [m] (used as unit distance, $d = 1$ m)
Elevation above sea level z [m]
Elevation Laplacian $\nabla^2 z$ [m^{-1}]
Global Geomorphic Energy GGE [kg.m^2.s^{-2}]
Glock's Available Relief GAR [m]
Gravity concordant change of PES determined by normal contour curvature $\Delta PES_{(k_n)_c}$ [kg.m^2.s^{-2}]
Gravity concordant change of PES determined by normal slope line curvature $\Delta PES_{(k_n)_s}$ [kg.m^2.s^{-2}]
Gravity discordant change of PES $\Delta PES_{(\tau_g)_c}$ [kg.m.s^{-2}]
Index of Connectivity IC [dimensionless]
Index of Slope Energy Disequilibrium $ISED$ [dimensionless]
Index of Gravity Discordant Energy Disequilibrium $IGDED$ [dimensionless]
Integral Potential Energy of Surface Curvature $IPESC$ [kg.m^2.s^{-2}]
Local Geomorphic Energy LGE [kg.m^2.s^{-2}]
Local relief (elevation differential in moving window) Δz [m]
Maximal curvature k_{max} [m^{-1}]
Maximum elevations a.s.l. / height of envelope (top) surface z_{max} [m]
Maximum Global Geomorphic Energy GGE_{max} [kg.m^2.s^{-2}]
Maximum Regional Geomorphic Energy RGE_{max} [kg.m^2.s^{-2}]
Mean curvature k_{mean} [m^{-1}]
Mean difference of Global Geomorphic Energy $\Delta\bar{G}GE$ [kg.m^2.s^{-2}]
Mean regional slope $\bar{S}$ [0.01% ≈ 0.00062831853071796 rad]
Melton Ruggedness Number MRN [0.01% ≈ 0.00062831853071796 rad]
Minimal curvature k_{min} [m^{-1}]
Minimum elevations above sea level z_{min} [m]
Normal contour (tangential) curvature $(k_n)_c$ [m^{-1}]
Normal slope line (profile) curvature $(k_n)_s$ [m^{-1}]
Potential Energy of Surface applicable to Diffusion $PESD$ [kg.m^2.s^{-2}]
Potential Energy of Surface applicable to mass flow PES [kg.m^2.s^{-2}]
Potential Energy of Surface excess PES_e [kg.m^2.s^{-2}]
Projected contour curvature $(k_p)_c$ [m^{-1}]
Regional Geomorphic Energy RGE [kg.m^2.s^{-2}]
Regional mean of PES $\bar{PES}$ [kg.m^2.s^{-2}]
Relative elevation/height above local base of erosion z_{rel} [m]
Relief Brake Force RBF [kg.m.s^{-2}]
Second slope line derivative z_{ss} [m^{-1}]
Slope aspect A [rad]
Slope inclination S [rad]
Specific catchment area a [m^2]
Stream Power Index SPI [dimensionless]
Supply of $\Delta PES_{(k_n)_c}$ from specific catchment area ΔPES_a [kg.m^2.s^{-2}]
Threshold of horizontality T_{hor} [rad]
Time t [s]
Topographic Position Index TPI [m]
Topographic wave amplitude w_a [m]
Topographic wave length w_l [m]
Topographic Wetness Index TWI [dimensionless]
Total accumulation curvature K_a [m^{-2}]
Total (Gaussian) curvature K [m^{-2}]
Unit Local Geomorphic Energy LGE_{unit} [kg.m^2.s^{-2}]
Volume of material V [m^3] (used as unit volume, $V = 1$ m^3)

1. Introduction

Geomorphological mapping plays an essential role in understanding Earth surface processes and geochronology, as well as the evaluation of natural resources and hazards (Bishop et al., 2012). Large scale geomorphological maps form the strongest scientific source of information and the best explanatory presentation of landforms and landscape development, but also serve as a basis of various applications (Gustavsson et al., 2006). However, subjectivism in the determination (selection) of mapped spatial units is a weakness of traditional mapping (e.g. as discussed by van Niekerk, 2010; Guilbert and Moulin, 2017; van der Meij et al., 2022). Hybrid approaches that combine expertise with statistical methods automate the translation of land surface attributes into spatial extents of the geomorphological features which were mapped by expert knowledge (Seijmonsbergen et al., 2011). This not only enhances the spatial precision of the end results but also accelerates the process of map generation in a reproducible manner. However, such procedures are complicated by the complex character of landforms and the ambiguity of many mapped units resulting in a great diversity of segmentation procedures and form descriptors.

By analysing these procedures, we attempt to show their mutual physical background arising from a physical interpretation of geomorphometric variables, which is the essence of the physical-geomorphometric approach.

In line with Giles (1998), Minár and Evans (2008) distinguished two basic approaches to elementary land surface segmentation: graph-based and classification approaches. The first is traditionally represented by 'morphological mapping' searching for slope discontinuities and other singular lines (breaks of slope, changes of slope and inflections) that can divide the territory into morphological units – plane facets and smoothly curved segments (Savigear, 1965). The slope units (half-basins) of Alvioli et al. (2016) are a recent example of a graph-based approach. Slope units are bounded by drainage and divide lines and can be considered elementary morphodynamic areas. Lastochkin et al. (2018) include both slope discontinuities and drainage and divide lines into their structural lines bounding elementary surfaces (convex, concave, or linear in profile and plan). In each of these approaches, mapping the boundaries is the priority and controls the character of delineated areas.

The classification approach is based on defining the internal properties of forms, from which the character of boundaries is derived. The simplest classification methods utilize concrete values of selected geomorphometric variables to define land surface segments (e.g. Hansen et al., 2021). Na et al. (2021) term such land surface segmentation a threshold approach. Curvature-based classifications are the most widely used example of this simplest classification approach, referred to by Krcho (1973) as geometric forms. If only convex and concave profile and

plan forms are distinguished (Troeh, 1964; Krcho, 1973), the boundaries are inflections (zero isolines of plan and profile curvatures, that are singular lines), connecting classification with graph-based approaches. However, adding linear geometric forms defined by a threshold small curvature (Krcho, 1979; Dikau, 1989) leads to the definition of form boundaries by arbitrary non-zero values of curvatures – not structural, but only arbitrary lines. Profile and plan curvature are in some classifications complemented by additional curvatures. In Wood (1996) widely used classification, complement of maximum and minimum curvatures define six forms (peak, ridge, pass, plane, channel, pit). Schmidt and Hewitt (2004) combine Krcho's and Wood's classifications defining 16 geometric forms. Shary (1995) used the 'complete system of curvatures' (plan, profile, Gaussian, difference, mean) to define 12 main types of land form, including Troeh (1964) as well as Gauss (1828) gravity invariant classification. Use of curvatures can be combined also with interval values of other geomorphometric variables. For example, Wood (1996) used a 'slope tolerance', and Krcho (1983) defined his 'morphotops' as a combination of geometric forms and interval values of relative elevation, slope, and aspect. Definition of the interval values can be (regionally) objectivized by a statistical measure such as hypsometric or clinographic maximums and inflections (Neto and de Souza Martins, 2019). Exclusively non-curvature variables have been applied only for regional (middle- and small-scale) segmentations (e.g. Neto and de Souza Martins, 2019; Cheng et al., 2011). Romstad and Etzelmüller (2012) applied the graph-based ('edge-based') approach on the only curvature: k_{mean}. The resultant 'mean curvature watersheds' are an alternative to the simplest geometric forms (Troeh, 1964; Krcho, 1973), where inflections as boundaries were substituted by extremum lines of the curvature. Another simple curvature (k_{max}) and its variability was effectively used for the terraces, landslide crowns and bank erosion detection, and found superior to a simple edge detector (Tarolli et al., 2012; Sofia et al., 2016). The methodological and interpretational simplicity of the curvature-based approaches is the reason for their persisting popularity. However, their use in geomorphological mapping is limited. The curvature-based approaches using only zero isolines as boundaries (Shary, 1995) ignore plains and linear slopes – fundamental elements of geomorphological maps. Using arbitrary slope and curvature thresholds for the definition of planar and linear forms leads to the rise of artificial (geomorphologically non-interpretable) boundaries of elementary forms. Moreover, distinguishing adjacent genetically distinct forms varying only in the magnitude of inclination or curvature is problematic in both cases (Minár and Evans, 2008).

More sophisticated statistical classification methods eliminate some of these limitations; however, they frequently sacrifice theoretical exactness. They are generally based on the geometric (or wider geomorphological) signature concept, originally assuming that the central tendency and dispersion statistics of different geomorphometric (geomorphological) attributes can distinguish geomorphologically disparate landscapes and landforms (Pike, 1988; Giles, 1998). Homogeneity of geomorphometric variables is most often considered, but their variability (e.g. McKean and Roering, 2004) or threshold values (e.g. Bolongaro-Crevenna et al., 2005; Xiong et al., 2017) are also used. The selection of concrete procedures for applying the approach should start from the specific purposes which the classification is to serve (Blaschke and Strobl, *2003*). The geomorphological signature is now understood statistically in greater complexity, and recent trends in land surface segmentation methodology are driven by progress in the fields of statistics, data mining, image processing and artificial intelligence (AI).

The core of these statistical methods is a kind of cluster analysis that already appeared in the land surface segmentation discourse half a century ago (Speight, 1974), and became a dominant methodological stream during the nineties (e.g. Irvin et al., 1997). Clustering algorithms minimise intraclass and maximise interclass differences, in accordance with the general requirement for land surface segmentation. However, their simple forms are based only on thematic similarity, ignoring spatial position (Minár and Evans, 2008), which frequently results in strongly pixelized ('pepper pot') results (e.g. Adediran et al., 2004). This is overcome (inter alia) by GEographical Object-Based Image Analysis (GEOBIA), which includes contextual and shape characteristics in the segmentation procedure. GEOBIA has been widely used in remote sensing since the beginning of the 21st century, and in the land surface segmentation of the last decade (e.g. Guida et al., 2016; Dekavalla and Argialas, 2017; Feizizadeh et al., 2021; Wei et al., 2021; Garajeh et al., 2022). It combines image processing and GIS functionalities in order to utilize spectral and contextual information in an integrative way (Blaschke, 2010). Substituting or combining the spectral image information with geomorphometric variables (Blaschke and Strobl, 2003; Drăguţ and Blaschke, 2006) became an efficient tool for land surface segmentation and classification.

Geostatistical methods simulating data patterns similar to a training area (e.g. the direct sampling presented by Giaccone et al., 2022) or various machine learning methods (e.g. Ding et al., 2021; Siqueira et al., 2022) also deal well with varied input data. They are a part of the most modern AI methodological stream. The encouraging AI approach in the realm of geomorphological mapping has been documented recently by leveraging deep machine learning, specifically Convolutional Neural Networks (CNNs) (Shumack et al., 2020; Li et al., 2020; Li et al., 2021; Meijles et al., 2022). CNNs are algorithms designed for pattern recognition on spatial or temporal data. These models learn from examples (annotated training sets) to associate pixel-level features with specific land surface classes. Because CNNs integrate spatial data generalization and segmentation, they can be perceived as a fusion of object-based and pixel-based mapping methodologies. In the comparative study of expert-driven and AI-driven methods by Meijles et al. (2022), CNNs performed well in identifying landforms, yet struggled with accurate delineation: hence the interference of a human geomorphologist was necessary for correction. Uncertainty in manual training and evaluation data sets impacted the CNN model performance, emphasizing collaborative mapping for quality assurance. The conclusion was that CNNs need further development and data processing to function independently as mapping techniques.

Older machine learning methods are also popular in experiments with land surface segmentation and classification. Other types of neural networks (e.g. Ehsani and Quiel, 2008; Foroutan et al., 2013) and random forest (e.g. Rabanaque et al., 2022; Na et al., 2021) are frequently tested. Supervised methods usually use training areas determined by experts for fine-tuning the model (e.g. Giles, 1998; d'Oleire-Oltmanns et al., 2013; Barbarella et al., 2021). Unsupervised approaches (purely data-driven segmentations) use a combination of predictor variables, seeking a segmentation approaching the targeted character. Most often they use simply the homogeneity of resultant units (e.g. van Niekerk, 2010; Piloyan and Konečný, 2017), alternatively the similarity to manually mapped units (e.g. Giaccone et al., 2022; Iwahashi et al., 2021), to a classification scheme (e.g. Rennó et al., 2008; Bock and Leyk, 2011) or to a dynamic interpretation (e.g. Guida et al., 2016). If different variables are used for the segmentation and for the subsequent classification, a combination of unsupervised (for the segmentation) and supervised (for the classification) approaches is possible (e.g. Anders et al., 2011).

Advanced statistical methods may seem to avoid the problem of selection of relevant input data. Robust statistics can deal with hundreds of randomly selected inputs: they are sorted out by the algorithm and only statistically significant inputs are finally used. Recent authors prefer using intuitively selected heterogeneous inputs (e.g. Garajeh et al., 2022; Giaccone et al., 2022) or inputs selected by robust statistical and data mining tools (e.g. Foroutan et al., 2013) prior to the theoretical reasoning. Targeted selection of inputs, however, is crucial for the theoretical exactness and interpretation of results.

The geometric signature concept uses only geomorphometric variables (Pike, 1988) while the concept of the geomorphological signature includes other data, typically from satellite imagery (Giles, 1998). The first can be theoretically analysed more easily (and improved in terms of

physical geomorphometry), in contrast to the second, which imitates traditional expert-based holistic identification of forms. Geometric approaches combining elevation, slope, aspect, and various kinds of curvatures are the most frequently used. Mainly in regional (small-scale) segmentations, however, elevation a.s.l. is sometimes substituted by relative elevation (relief), or Glock's Available Relief; the curvatures are regularly substituted by openness, Topographic Wetness Index (TWI), Topographic Position Index (TPI), or Stream Power Index (SPI). Unfortunately, the various concepts of land surface segmentation and classification are disconnected, and poorly integrated in terms of knowledge and analytical reasoning (Bishop et al., 2012). Very often, the application of descriptors used is not well reasoned in terms of theory. Automated classification of landforms usually attempts to replicate a previous prototype manual classification or mapping that has tended to use subjectively formulated differentiating criteria (MacMillan and Shary, 2009). Moreover, the selection of these criteria is frequently hampered by data and method accessibility (Minár et al., 2020).

Recently there has been a strong demand for systematic, theoretically based guidance of geomorphometric variable selection for each specific use (Franklin, 2020; Xiong et al., 2021; Maxwell and Shobe, 2022). Thus, the idea of experiments driven by the accessibility of data (and/or method) changes to experiments based on hypotheses arising from a theoretical assumption (Minár et al., 2020). The whole of land surface analysis for landform extraction should be based on the theory and principles of geosciences, mathematics, and computer sciences (Sofia, 2020).

Traditional determination of the extent and genesis of landforms is based on landform geometry and a set of other discriminant characteristics (rocks, soils, land cover, position, …). This corresponds to the geomorphological signature concept. Excessive diversity of identification attributes, and relationships between them, inhibits the theoretical unification of such approaches to segmentation. However, a large majority of all segmentation procedures contain a geomorphometric core: the set of input geomorphometric variables (geometric signature). Some of these have an unambiguous physical meaning, leading to various morphogenetic interpretations that should be part of a general theoretical framework of land surface segmentation. The concept of Minár and Evans (2008) seeking a theoretical synthesis of various geometric approaches to producing elementary land surface forms provides a starting point for building such a theoretical framework. Elementary forms are defined therein as segments with a tendency to a constant value (i.e. homogeneity) of 'gravity field-specific local geomorphometric variables' (Shary et al., 2005; Evans and Minár, 2011): altitude or its derivatives (slope, aspect, curvatures, and changes of curvatures) that are regularly bounded by discontinuity lines of these variables. Such elementary forms can be detected in the framework of a graph-based approach, looking for discontinuity lines (Pacina, 2009), or by a classification method searching areal homogeneity in altitude and its derivatives (Drăguţ et al., 2013), or by manually combining both approaches (Barka et al., 2011; Mentlík and Novotná, 2010). However, the heuristic assumption of full coverage of the land surface by homogeneous elementary forms ('contrast georelief' of Minár, 1992) is a weakness of this concept in which the main types of elementary forms are defined as equilibrium surfaces. This ignores the nonequilibrium or transitional patches of the land surface, which objectively exist and cannot be neglected (Li et al., 2020).

Definition variables for elementary forms are limited to the set of 'local, point-based variables, specific to gravity field', while many segmentation procedures include also other types of variables: 'local field-invariant', 'local area-based' and 'regional variables' (c.f. Evans and Minár, 2011). Linkages between point-based and important area-based and regional variables exist, but they have not been systematically investigated until now. Practical application of the concept of elementary forms, therefore, requires making a combination, with all these challenges: to deepen the theory of elementary forms and contextualize it in the framework of general geomorphological theory, enabling integration of the theoretical backgrounds of various segmentation procedures. This task mainly includes systematic physical interpretation of relevant geomorphometric variables (physical geomorphometry) and reflects a shift from the equilibrium to the non-equilibrium paradigm in research on geomorphic systems (Huggett, 2007). The geomorphic energy concept, rationalizing landform evolution (Devlin, 2003; Phillips, 2009; Lisenby et al., 2018), can play a key role also in land surface segmentation.

Based on the review of existing physical-geomorphometric approaches, this paper contributes to the theory of physically-based geomorphometry in order to improve land-surface segmentation and digital geomorphological mapping. Specifically, we systematize a new concept of geomorphic energy that interconnects elevation, slope and curvatures, and their changes. This concept enhances the definition of elementary forms, which will guide land-surface segmentation towards outputs that carry a better morphogenetic interpretation. The applicability of the new concept in an operational setting is demonstrated by an algorithm developed within the framework of Geographic Object-Based Image Analysis (GEOBIA). The elementary forms obtained through land-surface segmentation are compared below with expert-driven field geomorphological mapping.

2. Physical geomorphometry for land surface segmentation

Physical geomorphometry can be considered as the study of land surface geometry in terms of principles, practices, and concepts of physics such as dimension, energy, work, force, thermodynamics and equilibria. It emphasizes the physical interpretation (e.g. Krcho, 1973; Mitas and Mitasova, 1998; Shary et al., 2002; Florinsky, 2018), contrary to descriptive geomorphometry focused on descriptive statistics (Evans, 1972). Physical geomorphometry can provide theoretical evaluation and comparison of existing segmentation procedures; it can build a synthesizing physically-based elementary land surface segmentation. This can be achieved by interconnecting the landform time-space hierarchy with principles of landform development, the role of the form-generating geomorphic processes (their energy, forces and work) and the expression of these processes in geomorphometric variables. This physical interconnection of form geometry, recent processes, and landform genesis creates an essential bridge between the time scales at which we can observe geomorphic processes and the generally larger scales at which we seek explanations and forecasts (Kirkby, 1996).

The following paragraphs review and synthesize theoretical knowledge for solving the following principal questions (and resultant tasks) of land surface segmentation:

1) What kind of segments are we looking for and by what kind of input data do we define them? (Analysis of hierarchy of landform units and choice and adaptation of input land surface representation – DEM).
2) What evidence was used to establish the segments? (Analyse geomorphometric variables with respect to their physical-geomorphological interpretation and interconnections).
3) What are the optimal input variables for defining elementary forms? (Joining the structural hierarchy of landforms with the computational and interpretational hierarchy of geomorphometric variables and geosystem theory).
4) How can the selection, pre-processing, and processing of input variables lead to the most interpretable elementary forms? (Revision of the Minár and Evans (2008) concept of elementary forms and resultant workflow in the framework of GEOBIA).

2.1. DEM generalization and landform hierarchy

Many landforms are scale-specific (Evans, 2003). Various landforms of various sizes can be detected in the same place. Smaller landforms are embedded in bigger ones, creating a *nested size hierarchy of landforms*. A

nested hierarchy can result from the interaction of geomorphic processes of various genetic types, volumes and durations. For example, mass movement can form large deep-seated gravity deformations that are covered by a set of smaller runoff features subsequently forming on the same slope, such as gullies and their colluvial fans. However, a single process can simultaneously create a *genetically linked structural hierarchy of landforms*: elementary forms, compounded landforms, and land systems (e.g. Minár and Evans, 2008). For example, surface runoff generates a nested hierarchy of badlands, gullies, and gully slopes; the mass movement hierarchy is landslide fields, landslide blocks, and particular landslide scarps (e.g. Bufalini et al., 2021).

Landforms of various sizes and structural hierarchies are characterized by different geometric signatures in which various geomorphometric variables are comprised. It is inconceivable to detect the whole set of hierarchically different units by one segmentation procedure; determination of the targeted spatial and structural hierarchic level of the sought units is needed. Hence, optimal geomorphometric description (and identification) of forms of a specific hierarchic level requires either a specific DEM resolution (an explicit generalization of high-resolution DEM) or a specific window size for the computation of geomorphometric variables (an implicit generalization of the DEM) (Minár et al., 2020). However, sufficient DEM resolution, accuracy, and homogeneous spatial quality is a necessary condition, as documented by Mashimbye et al., 2014.

Elementary forms at detailed scales (e.g. MacMillan et al., 2000; Minár and Evans, 2008; Ehsani and Quiel, 2008; Gerçek et al., 2011) and land systems at regional or global scales (e.g. Drăguţ and Blaschke, 2006; Dekavalla and Argialas, 2017; Na et al., 2021) are mostly used in wall-to-wall (comprehensive) segmentations. Selective detection or mapping of predicted occurrence of only a single genetic type of form (e.g. planation surfaces, landslides, cirques, gullies, cryoplanation terraces, dunes) is also frequent in the recent discourse (e.g. Xiong et al., 2017; Sîrbu et al., 2019; Conoscenti and Rotigliano, 2020; Queen et al., 2021; Li and Zhao, 2022). DEMs of various resolutions and accuracies are used, but the determination of rules for the optimal DEM choice and adaptation is rarely considered (exceptions include Hengl, 2006; Lindsay et al., 2015, Woodrow et al., 2016; Xie et al., 2021; Popov et al., 2021; Newman et al., 2022). Implicitly, the DEM resolution should be harmonized with the size of particular genetic forms sought and/or the magnitude of form-forming processes. However, the relation between the event magnitude and its geomorphic effect is frequently non-linear (Lisenby et al., 2018; Gonzalez-Hidalgo et al., 2012): that complicates the 'a priori' setting of DEM resolution on the basis of process theory. Fortunately, highly detailed DEMs derived by airborne laser scanning or (in open/non forested areas) photogrammetry provide means for finding the optimal level of DEM generalization adopting the Nyquist-Shannon theorem. Terrain morphology in such DEMs is typically oversampled with respect to the level of scale intended for geomorphological mapping. Therefore, the optimal level of generalization (applicable spatial scale, i.e. spatial resolution) can be found as the balance between the minimum sampling interval for capturing the desired terrain features accurately and avoiding unnecessary DEM data redundancy while preserving the essential characteristics of the terrain.

Land surface segmentation has many alternatives: geomorphologists making manual segmentation select the most interpretable forms (e.g. Dramis et al., 2011; van der Meij et al., 2022). They prefer genetically clear, well-developed forms characterized by a kind of form stability and/or dynamic equilibrium, responding to the effective geomorphic extent of a form-forming process. They also limit the size of mapped forms, implicitly or explicitly selecting the scale of the resultant map and the minimum area of mapped units. Smaller forms are information noise. In simulating the geomorphologists' work, automatic segmentations are also supposed to detect only forms above a specific hierarchical level. DEM generalization can eliminate both DEM uncertainty and the noise resulting from the presence of undesired small (noise) forms. A specific task is to find the most suitable generalization level for the geomorphological interpretation of resultant segments (Popov et al., 2021). Depending on the character of resultant objects, various geomorphometric indices are used for explicit or implicit generalization of a DEM. The topographic grain (Pike et al., 1989) expresses the characteristic local ridgeline-to-channel spacing. A generalized DEM should preserve these important features thus the DEM resolution can be set up in line with the characteristic topographic grain. According to the Nyquist-Shannon sampling theorem (Hengl, 2006), to avoid aliasing the grid resolution should be finer (i.e. the cell size should be smaller) than half the average spacing between the inflection points on a transect. This corresponds to half of the topographic grain, but given the variability in grain, a considerably smaller spacing is likely to be suitable. The geomorphon concept based on the DEM openness attribute (Jasiewicz and Stepinski, 2013) contains an indirect generalization of a DEM by a look-up distance determining the maximum scale of a landform element; topographic grain has already been successfully used for this (Józsa and Fábián, 2016; Sărășan et al., 2019). Use of the theory of signal analysis can be a more robust alternative. A Fourier transform filter transforms a gridded DEM from the signal domain into a frequency domain, revealing basic land surface trends that represent a suitable generalization level (González-Díez et al., 2021).

Detecting appropriate landform scales from a DEM by local interpolation of landform surfaces at different window sizes was the solution offered by Schmidt and Andrew (2005). They used local scaling behaviour of surface approximations by second order polynomials in various window sizes, to identify dominant scale ranges and subsequently measure derivatives at those scales. Change of sign of plan curvature was used as the main indicator for the detection of various hierarchic levels. Hurst et al. (2012) evaluated the behaviour of the mean and standard deviation of "hilltop curvature" (elevation Laplacian) in various window sizes to determine a suitable length scale for curvature computation; this also represents implicit DEM generalization. As alternatives to standard deviation, measures of spatial autocorrelation (e.g. Moran's I) are also used for the determination of inter-segment heterogeneity (Na et al., 2021). This approach corresponds to the optimization of the grid resolution by maximizing its information content, as suggested by Hengl (2006). Maximization of the quantile-based measure of kurtosis K_0 of changes of curvatures (Minár et al., 2013b) also corresponds to this principle and was already successfully used for explicit DEM generalization to a level suitable for detection of elementary forms (Feciskanin and Minár, 2021; Popov et al., 2021). Introducing K_0 results from the specific properties of the targeted morphometric units (elementary forms), which is in line with the approach suggested by Louw and van Niekerk (2019) for scale optimization in multiresolution segmentation by GEOBIA.

Determination of the adequate level of generalization is only one aspect of adapting the DEM for successful segmentation. The selection of an appropriate generalization method is also important. A simple averaging or polynomial approximation, as prevails in current practice (e.g. Popov et al., 2021), is acceptable only for low degrees of generalizations. Hierarchical land surface segmentation requires a DEM generalization technique that also preserves the main topographic features at high levels of generalization. Grid-based DEM generalization methods have limited capabilities to meet this requirement, although promising solutions have been emerging lately (Lindsay et al., 2015, 2019; Newman et al., 2018, 2022). Therefore, many methods use other structures to create a generalized model. A common approach in land surface modeling is to extract 3D points (and lines) from DEMs using various techniques and use them to reconstruct the terrain surface using TINs (Zhou and Chen, 2011). Polygonal simplification methods, on the other hand, work directly on a polygonal (triangular/TIN) model; instead of the usual selection of model vertices, they use local modifications of the TIN (vertex clustering, vertex decimation, and edge collapse). The properties of the generalized model depend mainly on the conditions of local modification: some of them have suitable properties for land surface modeling based on the theory of the optimal triangle to

represent a smooth surface (Feciskanin and Minár, 2021). The generalization of a DEM based on this kind of polygonal simplification algorithm is theoretically well justified and preserves important topographic features very efficiently, even for high-level generalizations.

2.2. Geomorphometric representation of geomorphic forces, energy, and work

Potential gravity energy is directly reflected in topography. It is only one of the various kinds of energy that form the land surface (Devlin, 2003; Phillips, 2009), but it principally influences the application of kinetic energy of various geomorphic agents and thus gravity flows and diffusion processes. By contrast to other types of geomorphic energy, its general geomorphic effect can be easily conceptualized using the hierarchical system of interconnected basic geomorphometric variables (Fig. 1).

In the following text, the term *geomorphic energy* means the potential gravity energy of a unit volume (1 m^3) of material on the land surface. Parts of geomorphic energy, and their changes, are represented by various geomorphometric variables.

Global Geomorphic Energy (*GGE*) is characterized by the acceleration due to gravity g [$m.s^{-2}$] and can by defined on the earth's surface as:

$$\boldsymbol{GGE} = \rho.g.z.V \quad (1)$$

GGE is the unit gravity energy [$kg.m^2.s^{-2}$] of a unit volume of material ($V = 1\ m^3$) with density ρ in elevation z [m a.s.l.] and corresponds to constructive geomorphic work theoretically expended on uplift of this material to the given elevation from current sea level (Fig. 1). This energy is available to destructive subaerial geomorphic processes flattening the land surface towards sea level (the main or overall erosion base level). Substitution of z by $\boldsymbol{z_{max}}$ in (1) (where the window size corresponds to the topographic grain after Pike et al., 1989) yields the expression of maximal *GGE* ($\boldsymbol{GGE_{max}}$) that corresponds to the minimum past endogenous work preserved in the recent topography (Bandura et al., 2021).

Regional Geomorphic Energy (*RGE*) can be defined as a contextual energy available for the planation of the land surface to the level of the local base of erosion:

$$\boldsymbol{RGE} = \rho.g.z_{rel}.V \quad (2)$$

where z_{rel} is the relative elevation above a local base of erosion (Fig. 1). It is equivalent to HAND (Height Above Nearest Drainage) of Rennó et al. (2008). Excluding depressions below sea level, $z_{rel} \leq z$ and so $RGE \leq GGE$. The z_{rel} of water divides represents maximal *RGE* ($\boldsymbol{RGE_{max}}$): it corresponds to ***GAR*** – Glock's Available Relief (Glock, 1932) and can represent the minimum past exogenous work of a region preserved in its recent topography (Minár et al., 2018; Bandura et al., 2021).

Local Geomorphic Energy (*LGE*) can be defined by local relief Δz:

$$\boldsymbol{LGE} = \rho.g.\Delta z.V \quad (3)$$

where $\Delta z = z_{max} - z_{min}$ in a window. If the window size is determined by the topographic grain, $\Delta z \cong GAR$ and $RGE \cong LGE$. The ratio of Δz to the window size approximates the mean slope gradient ($\bar{S}$): for decreasing window size this approaches the tangent of local slope inclination (S).

GGE, *RGE*, and *LGE* are variants of the potential energy of mass transfers of Phillips (2009) – that means potential gravity energy of the unit volume of in situ material. Only a part of this energy can be directly used for geomorphic work. The following kinds of energy express the potential influence of topography on the distribution of the unit volume of moving material along unit distance ($d = 1$ m), where curvatures cannot exceed the value of 1 m^{-1}.

Potential local energy on the land surface applicable to mass flow (in short: Potential Energy of Surface – *PES)* is defined by Minár et al. (2020) as a function of the sine of local slope inclination S:

$$\boldsymbol{PES} = \rho.g.sin\ S.d.V \quad (4)$$

where $d = 1$ m is the unit downslope distance. Regarding a smooth surface, where $S \in [0°, 90°]$ and d, $V = 1$, the $PES \leq \rho.g = LGE_{unit}$, where LGE_{unit} is the unit Local Geomorphic Energy of $\Delta z = 1$ m (Fig. 1) and so:

$$\boldsymbol{PES} = LGE_{unit}.sin\ S \quad (4a)$$

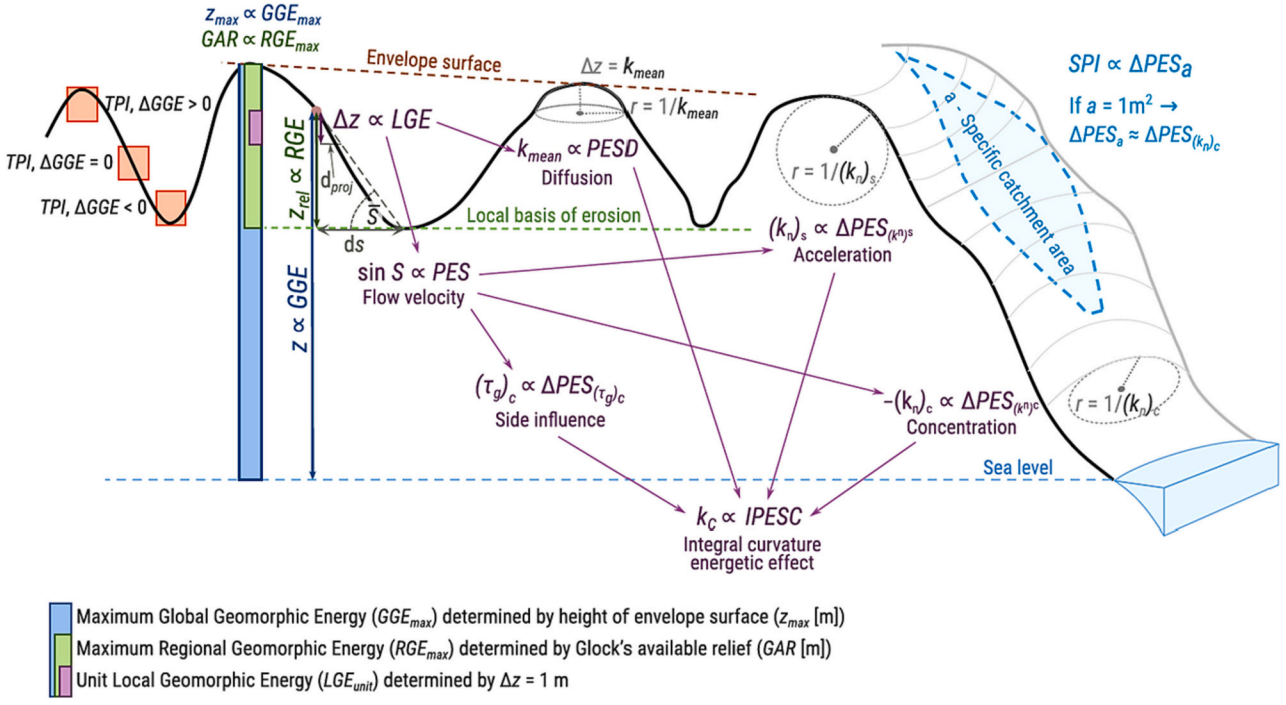

Fig. 1. Basic types of geomorphic energy defined by geomorphometric variables and relationships between them. Local Geomorphic Energy and its types are in violet. For more explanation, see the text.

The d in (4) is 3-D surface distance; its map projection (d_{proj}) is a function of S ($d_{proj} = d.\cos S$). The ratio of *PES* and d_{proj} thus expresses the projected *PES* distribution in the map that can be termed the 'projected *PES* density'(PES_{proj}):

$$PES_{proj} = \frac{PES}{d_{proj}} = LGE_{unit}.tanS \tag{4b}$$

The PES_{proj} expresses the apparent (projected) concentration of *PES*. It is only a projection of the real energy. If slopes reach 90° it has no physical meaning (tan S becomes infinite). Both *PES* (sin S) and PES_{proj} (tan S) are represented in various forms in many dynamic and evolutionary geomorphic models, where they are seemingly equivalent but only for gentle slopes. Derivation of PES_{proj} (4b) points to the physical interpretational priority of sin S over tan S, repeatedly mentioned in the literature (e.g. Strahler, 1952; Shary et al., 2002; Minár et al., 2020).

Gravity-concordant changes of PES include the direct influence of profile-normal slope line curvature $(k_n)_s$ and plan-normal contour line curvature $(k_n)_c$ on the mass flow (Minár et al., 2020, Fig. 1):

$$\Delta\boldsymbol{PES}_{(k_n)_s} = \rho.g.(k_n)_s.\mathrm{d.V} = \mathrm{LGE_{unit}}.(k_n)_s \tag{5}$$

$$\Delta\boldsymbol{PES}_{(k_n)_c} = -\rho.g.(k_n)_c.\mathrm{d.V} = \mathrm{LGE_{unit}}.-(k_n)_c \tag{6}$$

Both are originally expressed as geomorphic forces (kg.m.s^{-2}), but regarding the influence of this force along the unit downslope distance d = 1 m, they can also be considered extra kinds of unit geomorphic energy equivalent to a part of the LGE_{unit}. While the $\Delta PES_{(k_n)_s}$ determines acceleration (convex, +ve values of $(k_n)_s$) or deceleration (concave, −ve values of $(k_n)_s$) of mass flow, the $\Delta PES_{(k_n)_c}$ controls concentration (concave, −ve values of $(k_n)_c$) or dispersion (convex, +ve values of $(k_n)_c$) of the flow. Their summation defines the *PES* excess (PES_e) (Minár et al., 2020):

$$\boldsymbol{PES_e} = \Delta PES_{(k_n)_s} + \Delta PES_{(k_n)_c} = \rho.g.2k_d.\mathrm{d.V} \tag{7}$$

where k_d is the difference curvature of Shary (1995). While *PES* homogeneity expresses the equilibrium state of the land surface, PES_e expresses the disequilibrium, which can be quantified by the *Index of Slope Energy Disequilibrium* (*ISED,* Minár et al., 2020):

$$ISED[\%] = 100\frac{PES_e}{PES} = 50\frac{k_d}{sinS} \tag{8}$$

where *ISED* expresses the local percentage increase or decrease of *PES* due to land surface curvature.

All quantities (5) to (8) can take positive or negative values expressing increasing (+) or decreasing (−) of PES in the slope line direction. If (5) to (7) are considered as geomorphic energy, negative values represent negative geomorphic energy connected with a decrease of denudation and transport capacity.

Gravity-discordant change of PES is the *PES* change in direction of contours: it does not directly influence the mass flow in the given point. It can be defined using the principal representative of twisting curvatures – the third from the basic trio of land surface curvatures after Minár et al. (2020) termed therein as contour geodesic torsion $(\tau_g)_c$. Because $(\tau_g)_c = \frac{\partial S}{\partial c}$ (change of slope angle S in direction of contour c: Jenčo, 1992), $\frac{\partial(sinS)}{\partial c} = (\tau_g)_c.cosS$; the influence of $(\tau_g)_c$ on *PES* change in direction of c can be expressed (by analogy to (4) in Minár et al., 2020) as:

$$\begin{aligned}\Delta\boldsymbol{PES}_{(\tau_g)_c} &= \rho.g.\frac{\partial(sinS)}{\partial c}.d_c.V = \rho.g.\left|(\tau_g)_c\right|.cosS.d_c.V \\ &= \mathrm{LGE_{unit}}.cosS.\left|(\tau_g)_c\right|\end{aligned} \tag{9}$$

where d_c is the unit distance in the direction of the contour (d_c = 1 m). The sign of $(\tau_g)_c$ reflects only the direction of action of $\Delta PES_{(\tau_g)_c}$ not its value, therefore the absolute value of $(\tau_g)_c$ is used in (9).

Gravity discordance means disharmony between principal directions (defined by maximal and minimal curvature) and the gravity-principal directions (slope line and contour line). The $\Delta PES_{(\tau_g)_c}$ then expresses the part of *PES* change that does not affect actual local mass flows: it reflects a change in spatial (regional) organization of gravity-determined processes indicating the influence of an adjacent regulator of land surface development (Minár et al., 2020). Rivers and boundaries of different rock resistance or different geomorphic processes are the most common regulators of this kind, forming gravity disequilibria quantitatively reflected by the $\Delta PES_{(\tau_g)_c}$. Hence $\Delta PES_{(\tau_g)_c}$ is a local manifestation of a regional influence affecting the long-term evolution of the land surface and leading to a long-term local gravity disequilibrium. The relative importance of $\Delta PES_{(\tau_g)_c}$ can be expressed by analogy to (8) as an *Index of Gravity Discordant Energy Disequilibrium* (*IGDED*):

$$IGDED[\%] = 100\frac{\Delta PES_{(\tau_g)_c}}{PES} = 100\left|(\tau_g)_c\right|.cotS \tag{10}$$

The regional mean of PES ($\bar{PES}$) can be defined by analogy to *PES* (eq. 4), substituting the local slope S with the mean slope $\bar{S}$ determined by the ratio of z_{rel} and distance to the nearest stream (ds) (Fig. 1):

$$\boldsymbol{\bar{PES}} = \rho.g.sin\bar{S}\ .d.V = \rho.g.\frac{z_{rel}}{ds}.d.V \tag{11}$$

It is an equivalent of the areal Relief Brake Force (*RBF*) used in morphostructural segmentation (Minár et al., 2018; Bandura et al., 2021):

$RBF = \frac{g.(GAR \cong z_{max} - z_{min})}{2.ds}.unit\ mass(=1\mathrm{kg})$. However, the $\bar{PES}$ is defined for unit volume ($mass = \rho.V$) and expressed as geomorphic energy or work, thus the action of *RBF* per unit distance (d): $\bar{PES} \approx \rho.V.RBF.d$. The Melton Ruggedness Number (*MRN;* Melton, 1965) is equivalent to $\bar{S}$ computed for a specific catchment area (a) (Marchi and Dalla Fontana, 2005): $MRN = \frac{z_{max} - z_{min}}{\sqrt{a}}$. So *MRN* also approximates the $\bar{PES}$, which explains its fruitfulness in landform classification (e.g. Marchi and Dalla Fontana, 2005; Ilinca, 2021). If $\bar{PES} \cong PES$, the local and regional topography is in accord: discordance of $\bar{PES}$ and *PES* points to the existence of lower-order landforms disturbing the regional organization principle (e.g. landslides on valley slopes).

Supply of $\Delta PES_{(k_n)_c}$ *from a specific catchment area* (ΔPES_a) is another extension of the *PES* concept beyond the local scale (Fig. 1). $\Delta PES_{(k_n)_c}$ expresses the rise of *PES* from the concentration of material only from the immediate surrounding of a point. Regionally, however, the material (and energy) is accumulated from the whole specific catchment area (a) of the point and so:

$$\boldsymbol{\Delta PES_a} = f\left(\sum_a \Delta PES_{(k_n)_c}\right) \tag{12}$$

where f is a function expressing the expenditure of $\sum_a \Delta PES_{(k_n)_c}$ inside of a. After Gallant and Hutchinson (2011), a can be estimated by the integration of the projected contour curvature $(k_\mathrm{p})_c$ along the flow path. Because $(k_p)_c = (k_n)_c\ /\ sin\ S$ (Krcho, 1983) and regarding (12), a is equivalent to the integration of $\Delta PES_{(k_n)_c}\ /\ sin\ S$ and so:

$$\sum_a \Delta PES_{(k_n)_c} \cong \rho.g.a.sinS \Rightarrow \boldsymbol{\Delta PES_a} \cong \rho.g.SPI \tag{13}$$

where *SPI* is Stream Power Index resulting from Mitasova et al. (1996) in the form:

$$SPI = a^m.(sinS)^n \tag{14}$$

and m, n are experimentally or physically-based coefficients (making specific the function f in (12)). The form of *SPI* using *tan S* instead of *sin S* (e.g. Moore et al., 1988) is not suitable for expressing ΔPES_a. It yields similar results to (14) for common slopes, but for scarps (S → 90°) the *tan S* leads to a nonsensical infinite ΔPES_a. An important part of the ΔPES_a is expended in geomorphic work inside the specific catchment, rising

exponentially with the catchment area (a). Therefore, the frequently used linear form of $SPI = a.\,S$ (e.g. Conoscenti and Rotigliano, 2020) is also not suitable for the expression of ΔPES_a. Theoretically, the application of the log form (using *sin S* instead *tan S)* looks more suitable, e.g. $SPI = ln(1 + a.sinS)$ (c.f. Florinsky, 2017). Also the power function of a ($n = 1$ and $0 < m < 1$ in (14)) resulting from empirical experiments (e.g. Vandaele et al., 1996; Clubb et al., 2014) seems suitable. However, the form (14) is the most general, reflecting the stream power law, which is a 'nearly universal morphometric relation' (Venditti et al., 2020). Coefficients m and n theoretically depend on the catchment shape (more energy is lost in an elongated catchment than in a circular), but also on regional specifics of lithology or climate. Applications in various territories point to regional calibrations being necessary (e.g. Daggupati et al., 2013), limiting application of *SPI* for elementary land surface segmentation.

The Topographic Wetness Index (*TWI*, Beven and Kirkby, 1979) has a similar physical basis to *SPI*. Inversion of the slope function ($TWI = \ln(a / \tan S)$) allows for expression of the accumulation of material (water) instead of the energy itself. However, local homogeneity and differences in ΔPES_a are also reflected in *TWI* values and can explain the success of using *TWI* in some segmentations.

Interesting relations exist between these *PES* concepts and the popular Index of Connectivity (*IC*, Borselli et al., 2008). *IC* is ratio of an upslope (D_{up}) and a downslope component (D_{dn}). D_{up} is a function of upslope contributing area (a) and D_{dn} depends on distance to the local base level ($\sum_i d_i$, where d_i is length of the ith cell along the downslope path). Both D_{up} and D_{dn} depend on average slope gradient S ($\bar{S}$ in a for D_{up}; average slope of path $\sum_i \frac{S_i}{d_i}$ for D_{dn}) and on a "weighing factor" ($\bar{W}$; $\sum_i \frac{W_i}{d_i}$) interpreted alternatively as the C factor of the USLE model (Borselli et al., 2008) or as a roughness index (Cavalli et al., 2013). Neglecting factor W and substituting sin S instead tan S, D_{up} clearly corresponds to ΔPES_a and D_{dn} to $\frac{1}{\bar{PES}}$ on the downslope path. *IC* then corresponds to the sum of logarithms of ΔPES_a and $\bar{PES}$:

$$IC = log\left(\frac{D_{up}}{D_{dn}}\right) = log\left(\frac{\bar{W}.\bar{S}.\sqrt{a}}{\sum_i \frac{d_i}{W_i.S_i}}\right) \propto log\Delta PES_a + log\bar{PES} \quad (15)$$

Connectivity describes the sediment flux behaviour and application of *IC* is focused on various morphodynamic problems (Heckmann et al., 2018, Najafi et al., 2021). *IC* also has potential for detecting homogeneous geomorphological units (Crema and Bossi, 2017), but its clustering leads to typological more than elementary segmentation.

Potential local energy on the land surface applicable to diffusion (in short Potential Energy of Surface for Diffusion – *PESD*) can be derived by discretization of the diffusion equation (e.g. Martin and Church, 1997 and references therein):

$$\frac{\partial z}{\partial t} = \kappa\left[\frac{\partial^2 z}{\partial x^2} + \frac{\partial^2 z}{\partial y^2}\right] = \kappa.\nabla^2 z \Rightarrow \frac{\Delta z}{\Delta t} \approx \kappa.\nabla^2 z \quad (16)$$

where κ is the diffusion coefficient [$m^2.s^{-1}$], t is time and $\nabla^2 z$ is the elevation Laplacian. The $\nabla^2 z$ is an 'imitation'of mean curvature $k_{mean} = \frac{k_{max}+k_{min}}{2} = \frac{(k_n)_x+(k_n)_y}{2}$; if $S \to 0$ then $\nabla^2 z \to 2k_{mean}$ (Minár et al., 2020). Denudation Δh (responding to the local geomorphic work during Δt) is in the hilltop position equal to Δz (Fig. 2 a). From the setting $\Delta z = 1$ m (defining LGE_{unit}) and $2k_{mean} = 1 \Rightarrow \Delta t.\,\kappa = 1\ m^2$. The member $\Delta t.\,\kappa$ can be considered as the unit area ($Area = 1\ m^2$) for which the curvature $2k_{mean} = 1\ m^{-1}$ causes range of altitude $\Delta z = 1$ m: it determines the unit value of *LGE* (LGE_{unit}). A decrease of $\nabla^2 z$ (k_{mean}) results in a decrease of Δz and thus Δh.

Then *PESD* can be expressed as potential diffusion work responding to *LGE* ($\Delta z = \Delta h$) for the unit area ($Area = \Delta t.\kappa = 1\ m^2$), responding to k_{mean} value (Fig. 1 and Fig. 2 a):

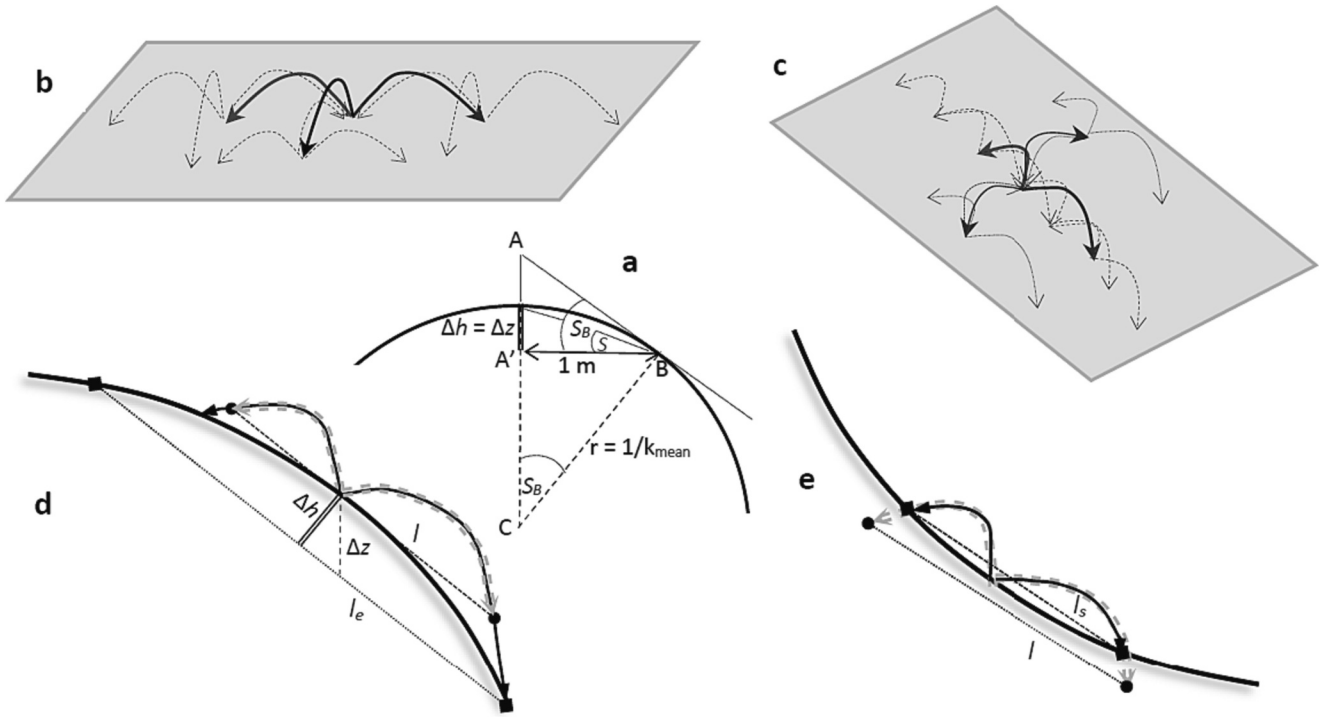

Fig. 2. Relationships of mean curvature k_{mean}, *PESD,* and the diffusion process: Hilltop curvature as a measure of *PESD* represented by Δh, where $\Delta h = \Delta z$ determines $LGE \approx PESD$ (**a**). Influence of the land surface on the diffusion dynamic: Omnidirectional movement is mutually eliminated on the horizontal plane (**b**) as well as on a linear slope (**c**). A convex slope elongates mean movement trajectories (le) in comparison with a linear slope (l), leading to a bigger dispersion of material and denudation (**d**). A concave slope shortens trajectories (ls), resulting in smaller dispersion and accumulation of material (**e**). The mechanism works in all compass directions.

$$LGE = \Delta z.\rho.g.V = \Delta t.\kappa.\nabla^2 z.\rho.g.V \Rightarrow \boldsymbol{PESD} = 2k_{mean}.\rho.g.\Delta t.\kappa.V \quad (17)$$

where $\Delta t.\kappa.V = 1$ expresses that it is part of the unit energy ($LGE_{unit} = \rho.g$) of a unit volume of potentially denuded matter spread on the unit surface area. Consequently, *PESD* can be defined also as a part of LGE_{unit} applicable to the diffusion of $Area = 1\ m^2$, determined by k_{mean} or (regarding eqs. (5), (6)) as the difference of gravity concordant changes of *PES*:

$$\boldsymbol{PESD} = LGE_{unit}.2k_{mean} = LGE_{unit}.\left((k_n)_s + (k_n)_c\right) = \Delta PES_{(k_n)_s} - \Delta PES_{(k_n)_c} \quad (17a)$$

The first part of (17a) is an analogy to the relation (4a) valid for the hilltop position. The average sine of slope S from the peak to the unit distance (1 m) corresponds to the curvature: $\bar{sin}S \approx 2k_{mean}$ (resulting from Fig. 2 a: the similarity of △ A A'B and △ A'BC and the relation $\bar{sin}S \approx 0.5 \sin S_B$). The maximum possible denudation $\Delta h = \Delta z$, thus *PESD* on the peak is equivalent to the *PES* in the immediate vicinity of the peak. Therefore so-called 'hilltop curvature' can well approximate the erosion rate also on hilltops with $S = 0°$ (Hurst et al., 2012), where from definition (4) the *PES* is zero.

On a slope, however, the maximum possible denudation resulting from the curvature is $\Delta h < \Delta z$ (Fig. 2 d) and so in the immediate vicinity of the peak $PESD < PES$. Moreover, $\nabla^2 z \neq 2k_{mean}$ and so only $\nabla^2 z$ or k_{mean} should be used for the general *PESD* definition. Recalling that mass transport rates may be related to the sine of the slope angle rather than the tangent (e.g. Martin and Church, 1997) and geometric $(k_n)_s$ (defining k_{mean}) is the change of sine of slope (Minár et al., 2020), k_{mean} is preferred in (17). As $\Delta h = \Delta z.\cos S$ and geomorphic work (denudation Δh) determined by *PESD* is projected in the map as Δz, the diffusion eq. (16) adequately describes the change of elevation a.s.l. with time (as used in evolutionary models), despite *PESD* being a function of k_{mean} and not of $\nabla^2 z$. Finally, by analogy to (4b), substituting k_{mean} with $\nabla^2 z$ represents the projection of the 3D *PESD* into 2D $PESD_{proj}$.

$$PESD_{proj} = \nabla^2 z.LGE_{unit} \quad (17b)$$

Diffusion best represents the set of geomorphic processes for which intensity directly depends on a single geomorphometric variable – the land surface curvature. Splash erosion is a typical example. Its intensity is zero on a horizontal plane and also on parts of variously inclined linear slopes, where shorter upslope and longer downslope movements of the material are mutually eliminated in the mass balance (Fig. 2 b, c). However, convex forms are denuded by diffusion, and the material is deposited on concave slopes (Fig. 2 d, e). The absolute value of diffusive geomorphic work (denudation and accumulation) depends on the effective external geomorphic energy of agents (raindrops in the case of splash erosion, wind in the case of windthrows, etc.). The unit value of this effective kinetic energy (1 $kg.m^2.s^{-2}$) is all spent on the particle movement, without a geomorphic effect on a horizontal plane and most of a linear slope (Fig. 2 b, c). The efficiency of denudation on a curved slope depends on the elongation of the mean trajectory on a convex slope; accumulation depends on its shortening on a concave slope (Fig. 2 d, e). The whole unit effective kinetic energy is spent on geomorphic work if the radius of curvature approaches the diffusion process extent (movement trajectory l). For a unit process extent ($l = 1$ m) this alternative dynamic definition of *PESD* is equal to the previous derivation of the *PESD* (17).

Integral Potential Energy of Surface Curvature (*IPESC*) can be introduced as a concept spanning the energetic influence of the basic trio of land surface curvatures ($(k_n)_s$, $(k_n)_c$, $(\tau_g)_c$) on land surface formation (Fig. 1). They determine changes in *PES* (5, 6, 9) and subsequently PES_e (7) and *PESD* (17a). Only the sign of $(k_n)_s$ has a straightforward physical-geomorphic meaning. Positive values of $(k_n)_s$ increase *PES* (PES_e) and *PESD*. Positive values of $(k_n)_c$ also increase *PESD* but decrease *PES* (PES_e); the sign of $(\tau_g)_c$ has no physical meaning. However, each kind of basic curvature potentially deforms the energetic balance on the land surface and any summation of their absolute values (expressing deviation from an equilibrium state represented by zero curvature) should have interpretational meaning. Casorati curvature $k_C = \sqrt{\frac{k_{max}^2 + k_{min}^2}{2}}$ measures the general curvedness of a surface, regardless of the sign of curvature (Koenderink et al., 2015), and is an expression of general non-linearity (Minár et al., 2020). If $(\tau_g)_c = 0$, $k_C = \sqrt{\frac{(k_n)_s{}^2 + (k_n)_c{}^2}{2}}$. Simultaneously increasing $\left|(\tau_g)_c\right| > 0$ increases the value of k_C. Therefore, k_C (integrating the influence of all three basic curvatures) can be used for the estimation of *IPESC* (as potential energy of unit $Area = 1\ m^2$):

$$\boldsymbol{IPESC} = \rho.g.2k_C.Area.V = LGE_{unit}.2k_C \quad (18)$$

IPESC in this form integrates the energetic influences of PES_e (7) and *PESD* (17) on geomorphic processes. On a gravity concordant land surface ($(\tau_g)_c = 0$) is valid: If $(k_n)_s = (k_n)_c$ then $PES_e = 0$ and $IPESC = |PESD|$. If $(k_n)_s = -(k_n)_c$ then $PESD = 0$ and $IPESC = |PES_e|$. If $\left|(k_n)_s\right| \neq \left|(k_n)_c\right|$, then $IPESC > PESD$ and $IPESC > PES_e$. However, for partial linearity (i.e. $(k_n)_s$ or $(k_n)_c = 0$) *IPESC* is bounded by $IPESC = \sqrt{2}|PESD| = \sqrt{2}|PES_e|$. This means the summary energetic effect of PES_e and *PESD* cannot exceed a $\sqrt{2}$ multiple of the larger of these two energies. In the case of gravity discordance, *IPESC* increases based on $\Delta PES_{(\tau_g)_c}$.

Mean difference of Global Geomorphic Energy ($\Delta\bar{G}GE$) is the difference between *GGE* at a point and the mean *GGE* in its surrounding (moving window):

$$\boldsymbol{\Delta\bar{G}GE} = GGE - GGE_{mean} = TPI.\rho.g.V \quad (19)$$

where $TPI = (z - z_{mean})$ is the Topographic Position Index (Weiss, 2001). $\Delta\bar{G}GE$ expresses the abundance or deficiency of geomorphic energy of the given point in comparison with its surrounding. Although $\Delta\bar{G}GE$ is derived from *GGE*, in principle it also expresses the local change of *RGE* ($\Delta\bar{G}GE \approx \Delta\bar{R}GE$); but $\Delta\bar{G}GE \neq \Delta\bar{L}GE$. In singular points (top, saddle and depression), the *TPI* approximate half of k_{mean} for window size = 1 and so (regarding 17):

$$\frac{4.\Delta\bar{G}GE}{window\ size} \cong PESD \quad (20)$$

The *Elevation percentile* (Gallant and Wilson, 2000), identical to the *Relative elevation* of Anders et al. (2015) also expresses the energetic position of a point but on a qualitative scale. Various '*Percent elevation*' measures of MacMillan et al. (2000) extend this expression from local to regional scales. Bathymetric position index suggested by Lundblad et al. (2006) has the identical energetic meaning as TPI, if z_{mean} is computed in the circle. Its variant, computing z_{mean} in the annulus (Moskalik et al., 2018) should return correlated, generally higher (more contrast) absolute values, however, its energetic meaning is less straightforward.

2.3. Geomorphometric variables, geomorphic units, landform development, and (geo)system theory

TPI and other positional geomorphometric variables are related to variability measures of elevation such as *Terrain Ruggedness Index TRI* of Riley et al. (1999), *Elevation standard deviation* (Evans, 1972; Xiong et al., 2017), and *Coefficient of variation* (Na et al., 2021). *The range of altitude* (Δz) defining *LGE* (3) also belongs to this family. All these are *local area-based variables* (Evans and Minár, 2011) expressing the variability of elevation (and so *GGE*) in a finite area. Changes of elevation over a vanishingly small area (derivatives) define *local point-based variables* (Minár et al., 2013a), that more exactly express various kinds of local gravity energy and the forces (*PES*, $\Delta PES_{(k_n)_c}$, $\Delta PES_{(k_n)_s}$, $\Delta PES_{(\tau_g)_c}$, PES_e, *PESD*, *IPESC*). They drive the actual local geomorphic processes (work), and they are used for the definition of most types of elementary geomorphic units (Fig. 3).

The mathematical hierarchy of local point-based variables is

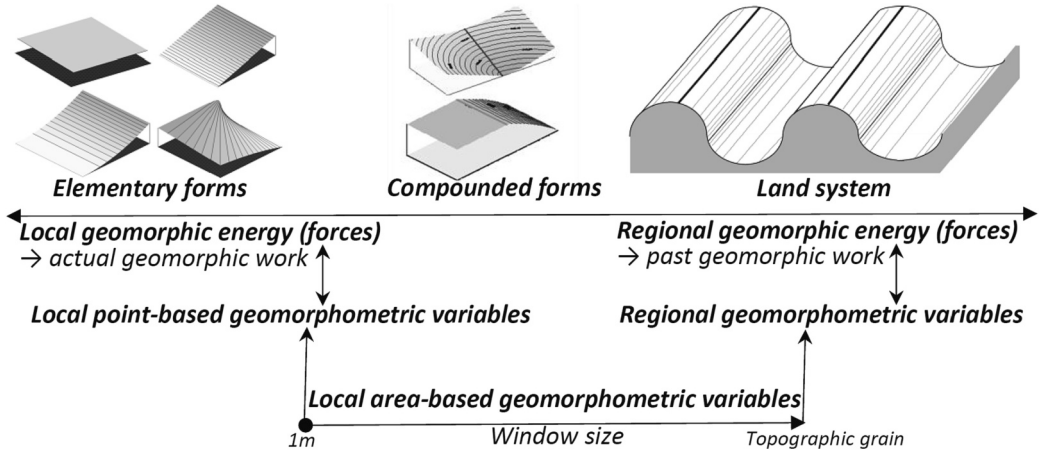

Fig. 3. Structural types of geomorphic units, driving energy and forces, and related groups of geomorphometric variables.

essential for segmentation. *Elevation z* is a variable of zero order and parent variable of all other variables defined by derivatives of *z* (slope, aspect, curvatures, and changes of curvatures). Because the derivative of a constant is zero, homogeneous (constant) elevation leads to zero values of all derived variables (and energies). First-order variables (*slope S* and *aspect A*) are parent variables of curvatures. Therefore, constant values of *S* and *A* lead to zero values of derived curvatures and changes of curvature. In reverse, looking for homogeneity in changes of curvatures, homogeneously low (zero) change of curvature means homogeneous (constant) parent curvature; homogenously low plan curvature means a tendency to constant aspect, and so on. This mutual support of local point-based variables in searching for homogeneous segments is fundamental to elementary land surface segmentation (Minár and Evans, 2008).

Global and regional geomorphic energy (*GGE*, GGE_{max}, *RGE*, RGE_{max}, $\bar{PES}$, ΔPES_a) well reflect past geomorphic work (Minár et al., 2018) and can be effectively used for identifying land systems (Fig. 3). They include traditional simple morphometric classifications (lowlands and highlands differentiated by elevation a.s.l.; plains, hill lands, … defined by relief and drainage density), as well as a recently published physically-based morphostructural segmentation (Bandura et al., 2021). The latter results from the conceptualization of topography as static waves whose energy is determined by wave amplitude ($GAR \propto RGE_{max}$) and length (reflected in the $\bar{S} \propto \bar{PES}$). It is compatible with the old concepts of local relief and topographic grain, expressing both as statistical quantities (Pike, 1988). ΔPES_a has a specific character. It expresses the regional influence on local *PES,* being a source of local disequilibrium but also (regionally) of equilibrial longitudinal profiles of rivers.

Local area-based geomorphometric variables significantly depend on the window size (Florinsky, 1998; Xiong et al., 2022). Some of them are associated with local point-based variables (expressing local geomorphic energy and forces) and with regional variables connected with regional geomorphic energy and work (Fig. 3). Δz coincides with $GAR \propto RGE_{max}$ (representing exogenous work) if the window size approaches topographic grain (Minár et al., 2018), but for a unit window size (1 m) $\Delta z \cong \tan S$, equivalent to the PES_{proj} (eq. 4b). In singular points, *TPI* approximates half of k_{mean} (quarter of *PESD*) for a unit window size and correlates with half of *GAR* (RGE_{max}) if the topographic grain is used. Openness (Yokoyama et al., 2002) is also related to k_{mean} in a unit window size; for topographic grain, it approaches the average slope defining $\bar{PES}$ or *RBF* (Minár et al., 2018; Bandura et al., 2021). These relationships lead to the similarity of frequently used classification schemes defined by various geomorphometric measures (curvature-based classifications of Krcho, 1983; Shary, 1995 and Wood, 1996, vs. openness-based classifications of Yokoyama et al., 2002 and Jasiewicz and Stepinski, 2013); also a mix of these measures can be effectively used (e.g. Walker et al., 2020).

Integration of physical and positional information is an advantage of some area-based variables (TPI, openness). However, local point-based variables are in theory more carefully formulated, clearly interconnected and hierarchized, and better interpretable physically. The effectiveness of their use in elementary land surface segmentation can be limited by computation from approximation polynomials with minimal freedom, from minimal computational windows, and using noisy, non-generalized DEMs. However, applying an adequate computational algorithm to a well-adapted DEM avoids that limitation: the resultant land surface segmentation can be interpreted effectively in terms of geomorphological development and (geo)system theory (Fig. 4).

Geomorphological mapping anticipates the existence of genetically distinct landforms, their spatial structures, and their associations (Evans, 2012). This would be inconceivable unless self-organization mechanisms existed in land surface development. Knowledge of the interplay of geomorphometric variables, geomorphic energy, and various aspects of self-organization should be reflected in the segmentation algorithm. The theory of landscape self-organization operates with energy dissipation, minimization, and maximization, considering the role of (dis)equilibrium and chaos for convergence towards some characteristic forms and divergence into diverse spatial mosaics (Phillips, 1999).

Convergence towards equilibrium elementary forms is at the core of the Minár and Evans (2008) concept. The geomorphological theory recognizes various types of equilibrium states that are attractors of land surface development, in various time extents. Davis' cycle of erosion is completed when the surface is lowered to a peneplain, minimizing Global Geomorphic Energy (*GGE*) during a cycle of tens of millions of years. Development of pediments and alluvial plains minimizes Regional Geomorphic Energy (*RGE*) in lower-order time-spans, and various horizontal (gently sloped) surfaces (e.g. structural or cryoplanation terraces) minimize local geomorphic energy (*LGE* and *PES*) at yet shorter times. It can be concluded that all horizontal planes ($z \cong$ constant) and low gradient surfaces ($z_{rel} \cong$ constant) are related to a *stationary state* characterized ideally by the absence of gravity-driven surface geomorphic processes. Disruption of this stability requires a strong external impulse (tectonic uplift, or incision of the base of erosion); typically, horizontal planes are only gradually degraded from the edge to the centre. Therefore *horizontality* is the strongest attractor of geomorphic development, with maximum persistence (time extent) and homogeneity (see green section in Fig. 4).

Minimization of energy and its dispersal (a general rise of entropy, in accordance with the 2nd thermodynamic law) is typical for physical self-organizing systems, including landforms (see blue section in Fig. 4).

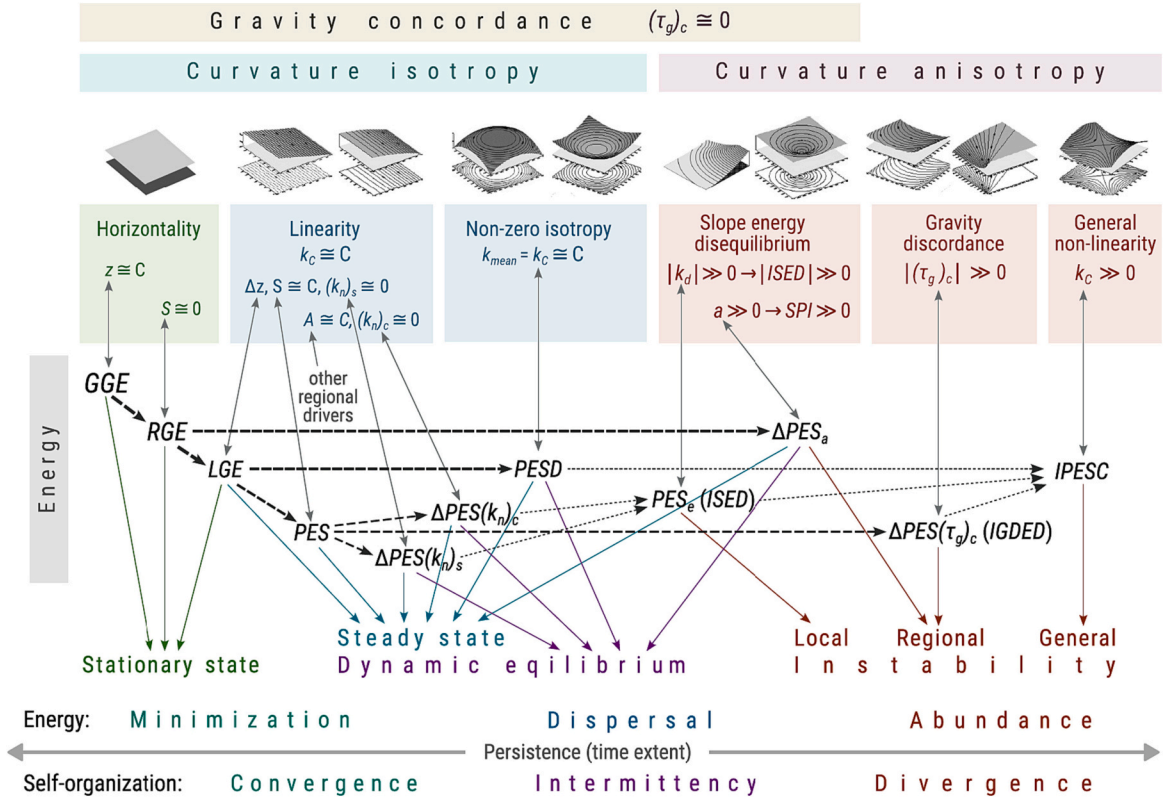

Fig. 4. Basic types of geomorphic equilibrium/disequilibrium and self-organization principles underlying geomorphic energy and geomorphometric expression. Dashed arrows: hierarchy of geomorphic energy. Double-headed arrows: definition dependence. Full single arrows: functional dependence. C – constant. Related categories are similarly coloured. For more explanation, see the text.

Linear slopes minimize energy and forces resulting from curvatures (*IPESC*) but the *linearity* is connected also with the uniform dispersal of *PES*. Both lead to the homogeneity of all local point-based variables derived from elevation, and frequently also to a steady state – a specific type of dynamic stability preserving the shape of landforms (Abrahams, 1968). Local minimization of $\Delta PES_{(k_n)_c}$ leads to the homogeneity of slope aspect (A), a parent variable of $(k_n)_c$. However, various regional drivers such as linear tectonic faults or prevailing wind directions also produce local uniformity of A. In gravity concordant forms, linearity in both gravity principal directions (constant slope and aspect) is linked with all curvatures having zero value, manifest in a zero value of Casorati curvature k_C. Alone, zero profile or plan curvature represents partial linearity with lower geomorphometric homogeneity and more complex conditions for dynamic stability. The simplest type is a combination of partial linearity in one direction with (non-zero) curvature homogeneity in the second direction. Non-zero curvature homogeneity in all directions corresponds to *non-zero curvature isotropy*. A part-spherical hilltop resulting from the linear diffusion equation is the best-known case (e.g. Small et al., 1999). It is conditioned by *PESD* (k_{mean}) dispersal (homogeneity): this applies, however, only on convex-convex and concave-concave forms (when $k_{mean} = k_C$). The resulting steady state was already proposed by Gilbert (1909) and some modern studies confirm its existence (e.g. Anderson, 2002). Non-linear diffusion models combining hilltop curvature isotropy with linearity in lower parts of the slope (e.g. Roering et al., 2001) can represent another kind of non-linear symmetry, where a transition zone could be characterized by a homogeneous change of curvature. With decreasing geomorphometric homogeneity, steady-state elementary forms are dwindling as development attractors. Non-steady state dynamic equilibrium does not involve any regularity of form (Abrahams, 1968) but usually preserves gravity concordance: parallel contours represented by zero twisting curvatures (Minár et al., 2020).

Curvature anisotropy is typical for a significant set of land surface elements (see brown section in Fig. 4). Disequilibrial landforms such as landslides, moraines, or badlands are built by catastrophic and turbulent processes related to dynamic instability and deterministic chaos. They are characterized by an abundance of local and regional geomorphic energy represented by slope energy disequilibrium ($PES_e \propto ISED$), gravity discordance ($\Delta PES_{(\tau_g)_c} \propto IGDED$) and general nonlinearity (*IPESC*). The abundance of any geomorphic energy can lead to *divergent land surface evolution*, differentiating landscapes into more diverse spatial units (Phillips, 1999), normally increasing the geodiversity (Gray, 2019; Chrobak et al., 2021). This occurs also during repeated self-organization towards a critical (threshold) high-energetic state (Phillips, 1999), which can be termed 'intermittency' (metastability), characterized by long periods of relative stasis (dynamic stability) and short bursts of activity (Smerlak, 2021).

2.4. Upgrading the concept of elementary forms

Based on the previous analysis, the input variables for elementary land surface segmentation should be directly linked with basic types of local geomorphic energy. This provides for the detection of segments characterized by minimization or uniform dispersion as well as a high abundance of these energies. In their concept of elementary forms Minár and Evans (2008) broadly respected this principle without, however, an exact definition of particular geomorphic energies, hence their system of geomorphometric variables for use was not exhaustive and optimal. It consisted of altitude (z), slope aspect (A), slope gradient (tan S), plan (projected contour) curvature ($(k_p)_c$) inverted as $R = 1/(k_p)_c$, profile curvature as the second slope line derivative (z_{ss}), plus derived third and higher order variables. Regarding Minár et al. (2020) and the analysis performed here, the following substitutions are suitable: tan $S \rightarrow$ sin S, $1/(k_p)_c \rightarrow (k_n)_c$, $z_{ss} \rightarrow (k_n)_s$ and subsequently a new set of third-order

variables (Fig. 5). Moreover, explicit incorporation of the principal representative of twisting curvatures ($(\tau_g)_c$) defining gravity discordant change of *PES* ($\Delta PES_{(\tau_g)_c}$) is desirable: Minár and Evans (2008) bypassed it by applying non-standard complex variables up to the 4th order.

Fig. 5 depicts the basic types of elementary forms of Minár and Evans (2008) defined by the set of local point-based variables. Excluding aspect *A* and Gaussian curvature *K*, all these variables up to second order directly represent the variants of geomorphic energy defined above: $z \propto GGE$, $\sin S \propto PES$, $(k_n)_s \propto \Delta PES_{(k_n)_s}$, $(k_n)_c \propto \Delta PES_{(k_n)_c}$, $(\tau_g)_c \propto \Delta PES_{(\tau_g)_c}$, $k_{mean} \propto PESD$. Aspect does not have a peculiar gravity-determined energetic meaning: it is, however, the parent variable of $(k_n)_c$, so its homogeneity means the absence (minimization) of $\Delta PES_{(k_n)_c}$. Moreover, its homogeneity can also reflect the homogeneous influence of a unidirectional physical field such as tectonic stress, solar radiation, or wind pressure. A horizontal plane – the most stable elementary form and biggest attractor – is in the left top corner of Fig. 5. Potential stability (and evolutionary attraction) decreases to the right and down, with the order of defining variables. All gravity-concordant elementary forms have a potential for dynamic equilibrium: curved segments less than linear facets. The opposite roles of $(k_n)_c$ in the definition of mass flow energy (PES_e) and diffusion energy (*PESD*) can prevent dynamic stability. It can be overcome simply in linear forms. Full linearity minimizes both, PES_e as well *PESD*. Partial linearity provides for equality of PES_e and *PESD* (if $(k_n)_c = 0$), or their complementarity (if $(k_n)_s = 0$), giving conditions for dynamic stability. From the non-linear forms, only isotropic spherical hills and depressions at once minimize PES_e and provide also for potentially uniform diffusion (dispersal of *PESD*). Dynamic stability of all other concordant forms requires preconditions that are more complex and unlikely, e.g. a continuous change of rock resistance.

Gravity-discordant elementary forms (bottom part of Fig. 5) are typically a manifestation of instability and transition states, as *PES* is unevenly distributed. In theory, linear-linear twisting slopes could have stability because *PESD* (k_{mean}) and PES_e ($\Delta PES_{(k_n)_c} = \Delta PES_{(k_n)_s} = 0$) are both zero. However, heterogeneous *PES* (given by non-zero $\Delta PES_{(\tau_g)_c}$) can be sustained long-term only by the influence of an external factor – e.g. a nearby dynamic regulator (river, fault activity, …) or by a change of rock resistance. Zero $\Delta PES_{(k_n)_c}$ and constant $\Delta PES_{(k_n)_s}$ on particular slope lines ($(k_n)_{ss} = 0$) can provide for uniform erosion, preserving the distribution of $\Delta PES_{(\tau_g)_c}$ on a slope with decreasing rock resistance in direction of contours. Any equilibrium of other gravity-discordant forms is yet more speculative. The 'diffusion-free' saddle with the equivalent plan and profile convexity/concavity ($(k_n)_s = -(k_n)_c \Rightarrow k_{mean} \wedge PESD = 0$) is not influenced by diffusion, but it is characterized by extreme contrast in $PES_{\underline{e}}$ – minimal on ridges and maximal on valley lines. This energetic imbalance can be compensated only by an external factor, in this case mainly by different rock resistance. Divergent development of the land surface is more probable, rather than any stability. Similarly, cylindric valleys and ridges have homogeneously diffused *PESD* (k_{mean} is constant), but $PES_{\underline{e}}$ is extremal along the axis (because $(k_n)_s = 0$, PES_e is minimal on ridge lines and maximal on valley lines). $PES_{\underline{e}}$ is increasing/decreasing towards valley/ridge sides. This is again a precondition of instability and divergent development: an incision of valleys and sharpening of ridges.

A set of other gravity-discordant forms can be defined by homogeneous derivatives of altitude in non-standard directions (Minár and Evans, 2008). Some of them have simple definition equations and are well represented by landforms such as a single landslide (consisting of simple concave denudation and convex accumulation sections), remnants of terraces, gravitational slump blocks (bottom-most forms on Fig. 5), multi-saddles (Peckham, 2011), and valley-ridge inflection points in which valley or ridge lines split into two branches (bifurcate); (Fig. 3 in Jenčo, 2018). However, their inner heterogeneity is clear – they resemble compounded rather than elementary forms. Also, significant heterogeneity of all kinds of geomorphic energy points to the instability of these forms. The presence of degenerate critical points defined by a zero determinant of the Hessian matrix (Jenčo, 2018) yet underlines their principal instability and development bifurcation. Identification of such forms in wall-to-wall segmentation is problematic, as they cannot be detected by the homogeneity of standard physically-based geomorphometric variables.

We thus suggest a set of standard physically-based geomorphometric variables up to third order (ringed in Fig. 5) for wall-to-wall land surface elementary segmentation. They are mathematically and physically interconnected, providing significant advantages. Clear physical meaning allows direct comparison and synthetic evaluation of variables. Regarding relations to LGE_{unit} (eqs. (3), (4a), (5), (6), (9), (17a)), the energetic equivalence of values of sine of slope and various curvatures can be postulated. Moreover, this energetic equivalence also concerns derived third-order variables. As a consequence, the summation, difference and ratio of energies defined by these variables (*LGE*, *PES*, $\Delta PES_{(k_n)_s}$, $\Delta PES_{(k_n)_c}$, PES_e,$\Delta PES_{(\tau_g)_c}$, *PESD*, *IPESC*) can easily be enumerated as a summation, difference, or ratio of the sine of slope, curvatures, and changes of curvatures multiplied by LGE_{unit}.

These mathematical relationships increase the effectiveness of the use of the whole set of variables in a segmentation procedure. Searching for uniformity of third-order variables also supports the detection of segments with low values of their parent curvatures (areas with minimum corresponding curvature energy). Uniformity of $(k_n)_s$ and $(k_n)_c$ supports the detection of forms with a low value of slope (*PES*); using slope as input also improves the detection of horizontal planes. In this way, the system is focused on searching for gravity-concordant elementary forms (upper part of Fig. 5), favouring delineation of the most geomorphologically important lower-order forms with the highest homogeneity and stability (Fig. 4). An arbitrary increase of the weight of lower-order input variables (elevation, slope, aspect) is an alternative. However, this frequently leads to over-segmentation (belts with similar altitude on steep slopes, or segmentation of homogeneous cones into various aspect sectors), which the use of third-order variables helps eliminate.

Incorporating twisting curvature ($(\tau_g)_c$) supports the detection of some gravity discordant forms (variously twisting slopes) but also of all gravity concordant forms (with $(\tau_g)_c \to 0$). Moreover, together with plan and profile curvatures $(k_n)_c$ and $(k_n)_s$ it completes the basic trio of land surface curvature from which all other curvatures can be derived (Minár et al., 2020). Three combined curvatures have also a clear energetic meaning ($k_{mean} \propto PESD$, $k_d \propto PES_e$, $k_C \propto IPESC$). In theory, their incorporation could also improve the discrimination of some forms, including some gravity-discordant forms such as saddle (without effective diffusion) and cylindric valley or ridge (Fig. 5). However, most gravity-discordant unstable forms are too complex and characterized not only by high values of any energy but also by high inner variability of this energy.

Detection of forms with high but very variable energy can be a problem for methods based on the maximization of inner homogeneity of input variables (such as GEOBIA). A transformation of input variables before the segmentation process can help. Normalization of input variables (reduction of the positive skewness of slope gradient and kurtosis of land surface curvatures) improves not only the reliability of parametric statistics (Csillik et al., 2015) but also favours homogeneity of segments in low energy realms and allows their higher heterogeneity in high energy areas. Inputs explicitly expressing the variability of geomorphic energy (based on elevation and its derivatives) provide alternatives for specific detection of such kinds of disequilibrium forms. E.g. McKean and Roering (2004) used the 'topographic surface roughness' expressing the variability of slope and aspect (i.e. *PES* and its changes) for detection of landslides. However, this is no longer elementary segmentation but the detection of disequilibrial compounded forms

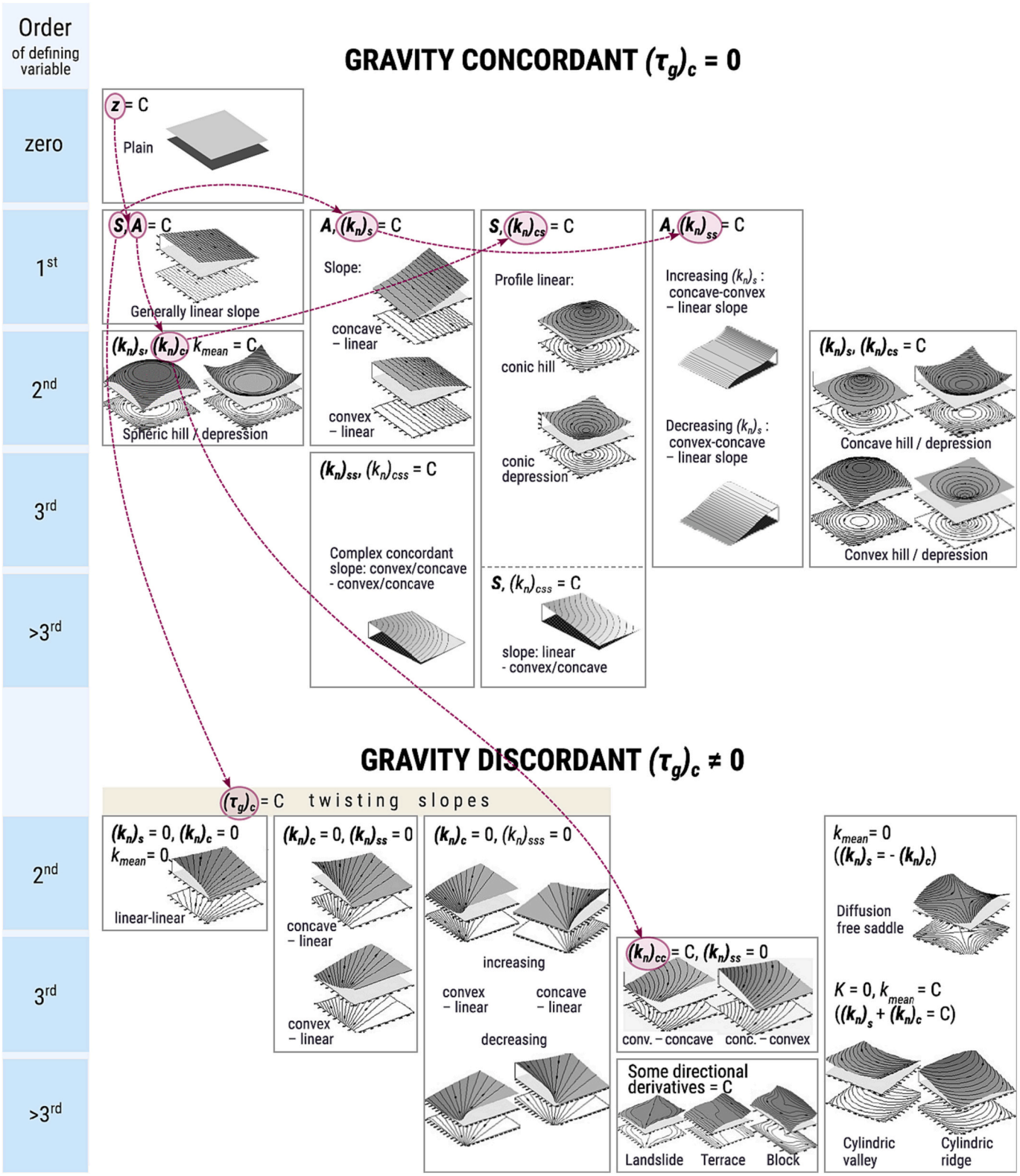

Fig. 5. Hierarchy and interconnection of geomorphometric variables and elementary forms: revised system of Minár and Evans (2008). Constant values (C) of variables define ideal types of elementary form and dispersal of corresponding geomorphic energy inside the form. Rings: interconnected variables up to third order, suggested for elementary segmentation; arrows express their definition and interpretation hierarchy. Third (and higher) order variables are marked as their parent curvature with an additional suffix expressing derivation in direction of slope line (*s*) or contour line (*c*). For more explanation, see the text.

(landforms).

2.5. Measuring affinity to ideal elementary forms

Investigation of the affinity of real segments to the ideal types of elementary forms from Fig. 5 is important for the interpretation of segmentation results. As an affinity measure, Minár and Evans (2008) used the function of unit average volumetric divergence between real segments and ideal models of elementary form. However, the divergence is always greater for a lower-order model than for a component higher-order model (constant change of curvature can approximate a slope better than constant curvature, constant curvature better than constant slope gradient, constant slope gradient better than constant elevation). No real segment has the highest affinity to the horizontal plane or linear slope in such a case. This makes a problem for geomorphological interpretation.

Variability of the input (form-defining) variables can provide an alternative measure of the affinity. Scown et al. (2015) used standard deviation (SD) and coefficient of variance (CV) of elevation and "total surface curvature" for evaluating the complexity of floodplains, related to their morphodynamic and morphogenetic particularities. If the ideal model of elementary form is represented by the mean value of the form-defining variable (sin S, $(k_n)_s$, …), the SD expresses some kind of normalized distance between the ideal model and real segment (analogous to the volumetric difference of Minár and Evans, 2008). It can also be perceived as the root mean square error (RMSE) of the real segment compared with the ideal type.

For comparability of the affinity of characteristics related to various geomorphic energies ($S \propto PES$, $(k_n)_s \propto \Delta PES_{(k_n)_s}$, …) one can normalize SD by the mean value of a characteristic (energy) representing the ideal elementary form. The resultant coefficient of variance (CV = SD/mean) expresses the 'relative' RMSE (difference of real segment from the ideal type), and because of the comparability of background geomorphic energies, it can be used for the comparison of affinity to various types of ideal elementary forms. For example, horizontal planes are characterized by the minimization of *PES* and linear slopes by uniform dispersion of *PES*. The same SD of slope gradient on a scarp and a very gentle slope is linked with a significantly lower CV in the first case and much higher in the second. Relatively small variation of the generally very high *PES* for a scarp means a strong affinity to a distinct steep linear slope (S = const.) with a tendency to dynamic equilibrium, but not to horizontality (z = const.). In the second case, the low values of slope gradient point to minimization of *PES* linked with a tendency to horizontality (and a stationary state), but relatively high CV (relatively low homogenization of the *PES*) excludes higher affinity to linearity. Because a CV takes extremely high values as the mean approaches zero, using CV is problematic in descriptive geomorphometry; however, it is meaningful in the case of physically-based affinity evaluation.

Generally, zero SD (as well as zero CV) of a variable related to energy means the total energetic homogeneity of the segment, at an average value describing a theoretically ideal elementary form (attractor). Non-zero CV then represents a deviation from this ideal state (how many times the variability of background energy exceeds its average, the ideal value). If the average is very low, a high value of CV suggests that affinity to a constant parent variable is more important (e.g. low average profile curvature points to a more important affinity to constant slope gradient). Therefore CVs of the slope, of all curvatures, and changes of curvature can be used as mutually compatible measures of segment affinity to the local attractor (i.e. homogeneity of the given variable and its related energy).

Affinity to an ideal elementary form is inversely proportional to the CV of the form-defining variable. For the simple comparability of convex and concave forms, absolute values of CV have to be used. We hypothesize that the mean of the form-forming variable (i) in a real segment represents an ideal elementary form (attractor) to which the development of the segment can tend. However, this role of the mean vanishes if the mean is too small in comparison with the standard deviation. We can establish a threshold: SD ≥ 2. mean as inadequate affinity and subsequently, we quantify affinity to the homogeneity of a morphometric variable i (Af_i) as follows:

$$Af_i = 1 - \frac{1}{2}\frac{SD_i}{|mean_i|} = 1 - \frac{|CV_i|}{2} \tag{21}$$

After (21), affinity is considered on the interval [0,1] and $Af_i \leq 0$ means NULL affinity. However, negative values of Af_i can also be interpreted as a measure of disequilibrium of the form in terms of variable i.

Two special cases are elevation (z) and aspect (A) affinity. CV of z (CV_z) represents the variation of Global Geomorphic Energy *GGE*, but *GGE* is much higher than Local Geomorphic Energy *LGE*, from which all other local energies (*PES*, *PESD*, Δ*PES* …) are derived. Therefore CV_z is much smaller than other CVs and applying (21) on all input variables, all segments have the biggest affinity to z = const. For comparability, the homogeneity of elevation should be evaluated by the medium of some local energy. That cannot be directly the *LGE* (represented by Δz) as Δz has no parent variable and if the average of $\Delta z = 0$, $CV_{\Delta z} \to \infty$, and so an ideal horizontal plane would have zero affinity to horizontality. However, instead of the mean value of Δz, an arbitrarily determined $\bar{\Delta z}_T$ can be used in (21). Let T_{hor} be the threshold of horizontality and an ideal linear slope with $S = T_{hor}$ have half affinity to the horizontal plane ($Af_z = 0.5$). Then $|CV|_T = 1$ and $\bar{\Delta z}_T$ has to be equal to the unbiased estimation of standard deviation:

$$\bar{\Delta z}_T = SD_{z_T} \approx \sqrt{\left(\frac{1}{3.46} tanT_{hor}.l_{ds}\right)^2} \cong \frac{tanT_{hor}.\sqrt{segment\ area}}{3.46} \tag{22}$$

where l_{ds} is the downslope length of the surface and $l_{ds}{}^2$ can be approximated by the segment area. Subsequently, a variable analogous to the CV of other variables (CV_z^*) can be derived:

$$CV_z^* = \frac{SD_z}{\bar{\Delta z}_T} = \frac{3.46.SD_z}{tanT_{hor}\sqrt{segment\ area}} \tag{23}$$

Eq. (23) returns $CV_z^* \approx 1$ for a linear, and in the plane ideal, compact (circular) segment with $S = T_{hor}$ and $SD_S = 0$. The shape of the segment influences the results: equally sloped segments elongated along slope lines (including ridges and valley bottoms) have lower CV_z^* than segments elongated along contours (terraces).

Aspect A is a circular quantity for which CV has no physical meaning. To avoid problems of directional statistics, both, sin A and cos A are used as inputs in segmentations (e.g. Drăgut and Blaschke, 2008; Drăguţ et al., 2013; Amatulli et al., 2018). Because A expresses the direction of S, and affinity to aspect linearity (A = const.) is exceeded by horizontality for $S \to 0$, the average value of sin S ($\bar{sin}\ S$) can be used also for the determination of CV_A*:

$$CV_A^* = \frac{SD_{sinA}}{\bar{sin}S} \tag{24}$$

3. Physically-based elementary land surface segmentation in GEOBIA: a worked example

An algorithm to demonstrate the concept of geomorphic energy has been designed using the multiresolution segmentation technique (MRS) implemented within the Trimble eCognition® software. MRS creates objects from adjacent raster cells that have similar values (Baatz and Schäpe, 2000). The size of the objects depends on a homogeneity threshold called scale parameter (SP), which can be determined in an objective manner (Drăguţ et al., 2010). Here we employed an automatic version of the Estimation of Scale Parameters (ESP, Drăguţ et al., 2014), which produces three scale levels of segmentation from detailed (L1) to broad (L3), based on the concept of Local Variance (Woodcock and

Strahler, 1987). Additional settings optimize the shape of the resulting objects (Shape parameter) by favouring either the compactness of the objects (Compactness), or the smoothness of their boundaries (Smoothness).

3.1. Territory and DEM adaptation

Sandberg hill at the contact of the Carpathians and Vienna Basin, Slovakia (Fig. 6 a) provides a pilot application of the theoretical concept presented above. The territory (0.25 km^2 in area) is a part of the man-made detailed geomorphological map of Minár and Mičian (2002):

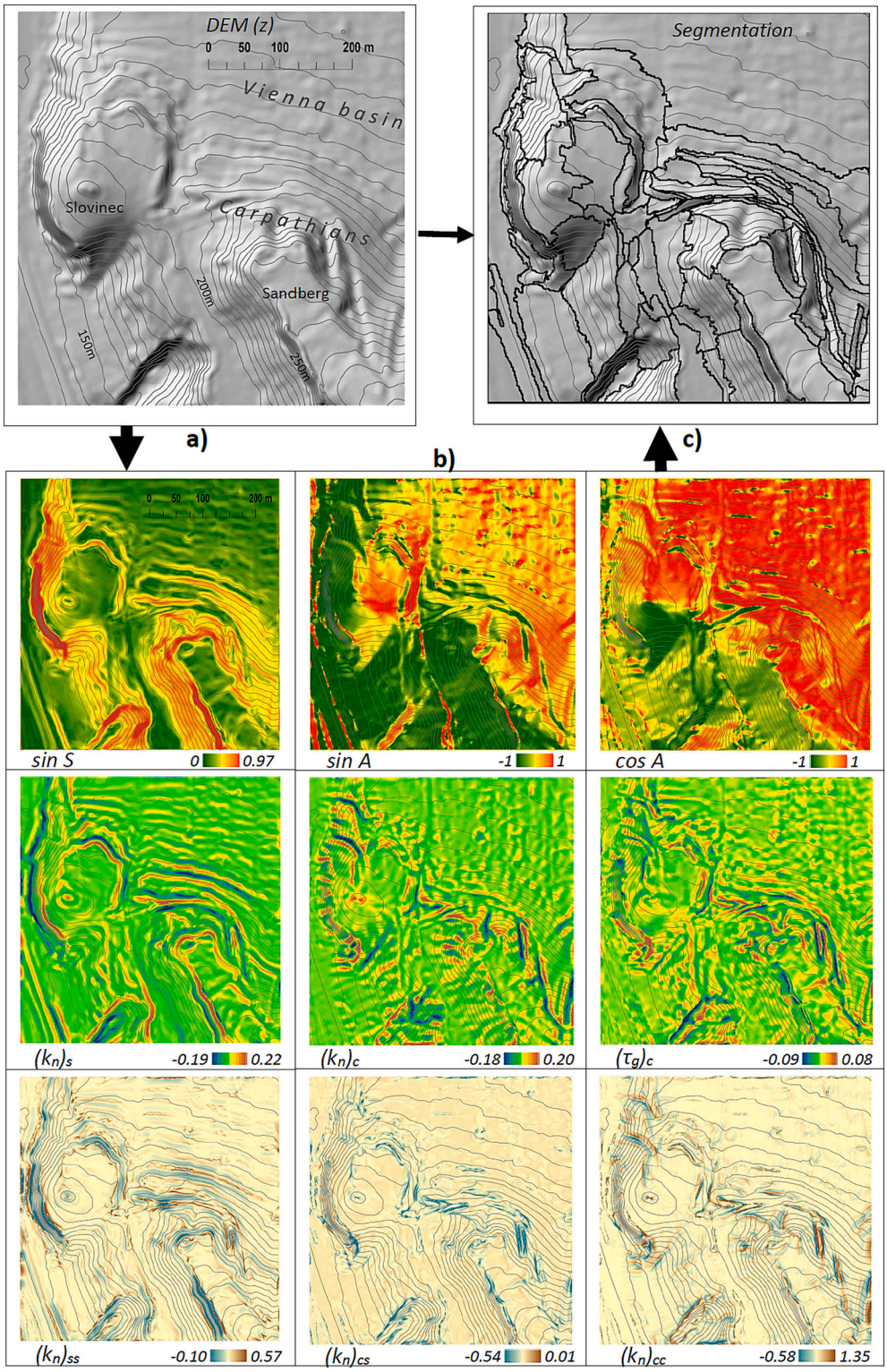

Fig. 6. Segmentation of Sandberg hill: **(a)** Input DEM. **(b)** Other inputs for GEOBIA generated from the DEM: goniometric functions of slope gradient *S* and aspect *A*; normal slope line curvature $(k_n)_s$; normal contour curvature $(k_n)_c$; basic twisting curvature $(\tau_g)_c$; change of $(k_n)_s$ in slope line direction $(k_n)_{ss}$; changes of $(k_n)_c$ in slope line and contour line directions $(k_n)_{cs}$, $(k_n)_{cc}$. **(c)** Segmentation used for geomorphological interpretation (Figs. 7, 8).

part of it (Slovinec hill, ~0.1 km^2) was used as a test area in previous stages of development and application of the elementary form concept (Minár and Evans, 2008; Pacina, 2009; Drăguţ et al., 2013; Minár et al., 2015). The local geology comprises Mesozoic limestones, Neogene sand and sandstone, and Pleistocene and Holocene fluvial and slope deposits. The Quaternary tectonic uplift of the territory determines the high geodiversity of this site. Ancient fortification and intensive modern land use resulted in significant anthropic modification of the land surface. Consequently, this complex territory comprises many landforms of varied geometry, order, genesis, and age.

Our previous work (Drăguţ et al., 2013; Minár et al., 2015) showed that the accuracy and level of the DEM detail are crucial for the successful segmentation of a complex territory. An airborne unclassified LiDAR point cloud (declared mean vertical error: 0.07 m) was used to generate a fine-scale initial DEM. Ground points were filtered from the last returns using the Cloth Simulation Filter (Zhang et al., 2016). The filter parameters differed in parts distinguished by land cover (vegetation, built-up area, grassland, rocky areas). Small holes without enough ground points were filled based on Poisson surface reconstruction (Kazhdan et al., 2006). The ground points formed vertices of a polygonal (triangular) model (with ~2,000,000 triangles). The basis for generating the input 1 m resolution DEM raster for analysis was a generalized polygonal model (with 500,000 triangles) generated by Quadric Error Metric Simplification (Garland and Heckbert, 1997).

In line with theoretical assumptions (Fig. 5), elevation and nine other local point-based variables up to third order were used for the segmentation (Fig. 6 b). As the third-order derivatives are very sensitive to noise in the data (Florinsky, 2009) we developed a procedure to determine the appropriate level of DEM generalization. In modification of Minár et al. (2015), directional partial derivatives up to third order were computed in the MATLAB environment by the least squares method (Florinsky, 2009), using a fourth-order polynomial and window sizes from 5 × 5 pixels (m) up to 25 × 25 pixels. Subsequently, three curvatures ($(k_n)_c$, $(k_n)_s$, $(\tau_g)_c$) (using equations given in Minár et al., 2020) and three changes of curvatures ($(k_n)_{cs}$, $(k_n)_{cc}$, $(k_n)_{ss}$) (equations in Minár et al., 2013b) were computed for all 20 variants of window sizes. Their K_0 indexes, kurtosis, standard deviations, and Moran's I were subsequently used to ascertain the suitable generalization level. The first mutual threshold was detected on the generalization level 9 × 9 pixels using graphs of dependence between the window size and the mean values of K_0, kurtosis, standard deviations, and Moran's I. Besides curvatures and their changes, slope and aspect were derived from the same DEM generalized in a 9 × 9 window. The sine of slope shows a bi-modal distribution of values that corresponds to the flat and sloping areas. Because of the circular character of aspect data, sine and cosine of aspect were used. Curvatures and their changes were transformed to approximate Gaussian distributions using the tool created by Csillik et al. (2015). Finally, all layers were normalized to the range 0–255 to avoid random weighting caused by the different types and ranges of the data.

3.2. Segmentation and digital geomorphological maps

The 10 layers were segmented with MRS in two steps. The first segmentation aimed at defining the flat objects in the scene, thus sine and cosine of aspect were not employed (both were assigned zero weights). The sine of slope was double weighted as compared to curvatures and their changes. The ESP was run with the default settings and a Shape parameter of 0.1, thus largely ignoring shape optimization and focusing on the statistical properties of the land surface (Drăgut and Blaschke, 2008). The value of Compactness was set to 0.5. Resulting objects with mean normalized slope values equal to or lower than 215 were separated as (relatively) 'flat'. That value separates the two modes in the slope histogram (note that this is after sine-transform and normalization to range). These flat objects were excluded from further processing, according to the concept of geomorphic energy. The second segmentation was run on the sloping objects using the same segmentation settings. All layers (including sine and cosine of aspect) were assigned normal weights (1) except for the sine of slope, which was doubled again.

Because the shape parameter was minimized in segmentation, several objects resulted in unnatural geometries. These objects were selected based on the geometry indices, as follows: objects with Shape Index ≥ 2.5 OR Compactness ≥ 2.5 OR Border Index ≥ 2.5 were first separated as geometrically anomalous. Objects with Density < 1, which may represent elongated features (e.g. valleys, ridges), were excluded from this class. The anomalous objects were refined with the "Shape Split" function, in 25 iterations. This function splits the objects based on the shape of their border, trying to adjust the geometry to "optimal" shapes. From the resultant three scale levels of segmentation, the middle level (L2) was used for the subsequent geomorphological analysis, based on having the closest comparability with the man-made geomorphological map of Minár and Mičian (2002).

Segmentation (basic differentiation of the territory) is only the first step of the geomorphological analysis. Field verification of elementary forms, their genetic interpretation, identification of compounded forms, and systemization (synthetic outlining of geomorphic development) are subsequent tasks (Mentlík et al., 2006). Linkage of the geometric, physical, and geosystem content of elementary forms with their genesis is fundamental and can be performed using the set of analytical maps (Fig. 7).

The geometric type of elementary form (Fig. 7 a) was defined by maximum affinity (Fig. 7 b) to one of the following ideal elementary forms: z = const.; S, A = const.; S, $(k_n)_{cc}$ = const.; S, $(k_n)_{cs}$ = const.; A, $(k_n)_s$ = const.; A, $(k_n)_{ss}$ = const.; $(k_n)_s$, $(k_n)_{cs}$ = const.; $(k_n)_{ss}$, $(k_n)_{cs}$ = const.; $(\tau_g)_c$, $(k_n)_s$ = const.; $(\tau_g)_c$, $(k_n)_{ss}$ = const. The affinity was computed using relations (21), (23) and (24) with setting $T_{hor} = 0.2$ rad (≈11.5°).

High affinity points to an equilibrium state related to the minimization or dispersal of *PES*, *PESD* and/or changes of *PES* (Fig. 4). Low maximal affinity points to general instability, related to the various kinds of local potential geomorphic energy (Fig. 7 c, d, e, f, i) and expressed by disequilibrium indexes (Fig. 7 g, h). Indices of instability can be interpreted in terms of catastrophic and anthropogenic form-forming processes and/or various transitional states. Examples from the following regional analysis explain these basic principles in more detail.

Automatically detected elementary forms cover all those mapped by Minár and Mičian, 2002 (Fig. 8 a), specifying their boundaries in more detail, dividing them into meaningful genetically distinct subparts and revealing also a set of distinct anthropogenic and erosional forms of lower order. Two digital morphogenetic maps were compiled interpreting the physical-geomorphometric content of elementary forms in the light of older research (Minár and Mičian, 2002; Minár et al., 2003) and additional field research. The first map abstracts the influence of human activity, assigning elementary forms to bigger units of natural geomorphic development (Fig. 8b). The second map depicts distinct anthropic forms and significant anthropization of natural landforms (Fig. 8c). This differentiation of morphogenetic forms into elementary forms is genetically meaningful. Every specific elementary form can thus be interpreted in the framework of the geomorphic development of the territory.

The oldest (Pliocene) land surface is represented by the flat top of Sandberg (segments 2, 3), interpreted as a regional pediment – 'river-side level' (Minár et al., 2004), protected by strong layers of resistant sandstone. A gentle structural slope (segment 1) separates it from a higher (older) pediment (outside the map). The low affinity of (1) to an equilibrium elementary form (a linear slope) is a consequence of structural steps inside the form. Structural steps, visible in Fig. 6, are contained also inside the main segment of the 'river-side level' (2) that is changed by early Medieval fortification leaving disequilibrium remnants of ramparts and ruins. It probably contributes to this segment having the smallest maximal affinity to an ideal elementary form (Fig. 7b). A small

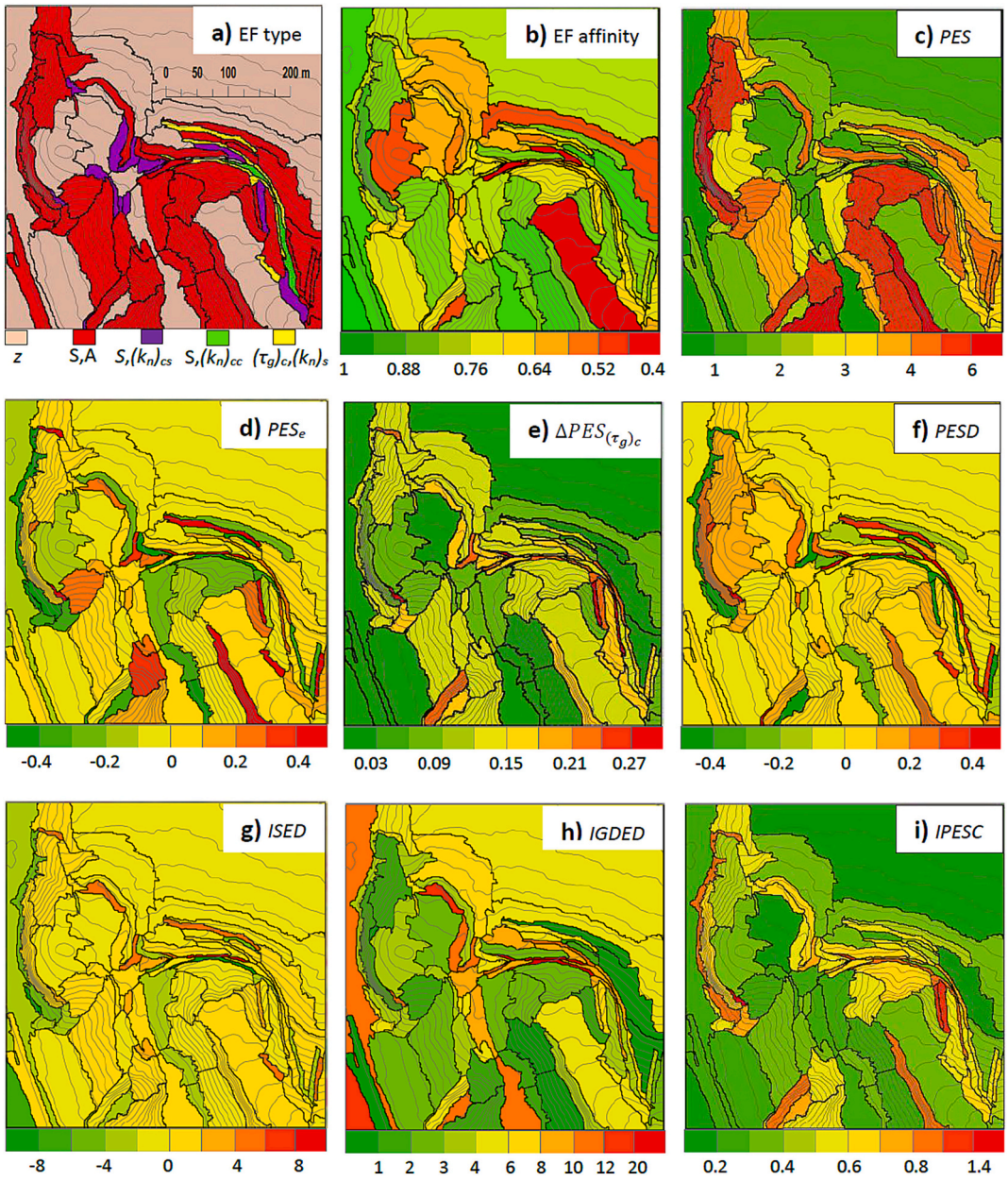

Fig. 7. Physical-geomorphometric analysis of Sandberg hill: Type of equilibrium elementary form (EF) with maximal affinity (a) and affinity magnitude (b) expressed by relationship (21), (23) or (24). Partial unit geomorphic energies (c, d, e, f, i) expressed for a unit body of water ($\rho = 1000$ kg.m^{-3}) in kJ. Disequilibrium indexes ISED (g) and IGDED (h) expressed in % of *PES*.

segment (3) represents a preserved natural transition of the planation surface to the fault slope.

Older fault-landslide slopes (segments 4–21) were formed after tectonic uplift (by about 50 m) around the Pliocene – Pleistocene boundary. Their formation was accompanied by the activation of block landslides. These differ in the character and magnitude of degradation. In the prevailingly sandy NW part, small blocks protected by thin sandstone plates form a strongly eroded dissected segment (17). Segment 18 differs from 17 by subsequent excavation – being used once as a local sand pit-quarry. The older SW fault-landslide slope reveals thick sandstone layers that were mined during the first half of the 20th century, reforming the slope into an industrial quarry. The quarry now consists of the quarry cliff (segment 20) and talus slope: the north part with only minimal recent activity of gravity processes (segment 19), and the south part (under the highest cliff) that is already very active (segment 21). The SE part of the slope is better preserved. Long homogeneous landslide scarps are elongated NNW-SSE in line with the master fault (segments 9, 13, 16). Asymmetric erosional valleys and gullies start below scarps (e.g. segments 14, 15). Ancient ramparts on the landslide block boundary (10, 6) influenced the formation of subsequent gullies and dells (12, 5) and slopes between them (11, 8). All anthropogenic features (and a majority of related segments) are characterized by lower affinity to an ideal elementary form and more extremal curvature energies and indexes (Fig. 7).

Segments with affinity to horizontality rim the foothills of the older fault-landslide slopes. Minár and Mičian (2002) interpreted them as partly an Early Pleistocene cryopediment (exhuming an abrasion platform) and partly a quarry flat. Analysis of the segmentation results points to the mutual initial genesis of segments 22–44 as a polygenetic planation surface. The flat of the former industrial quarry (23) is an erosion surface on the Miocene sands, only slightly transformed by the quarry deposition (up to 1 m). The flat (27) below a local sand pit-quarry

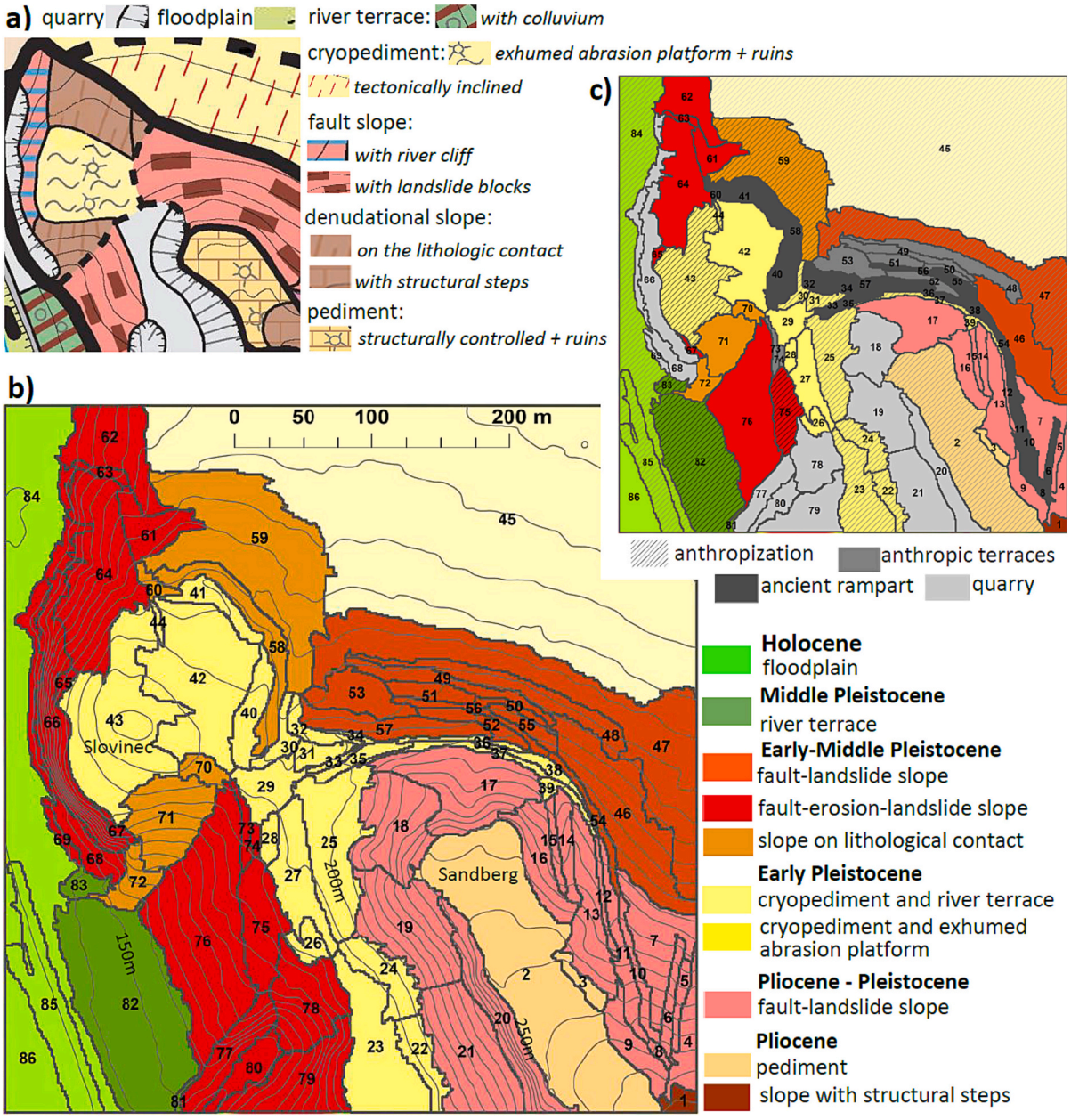

Fig. 8. Geomorphological mapping of Sandberg hill. **a**) Man-made geomorphological map (Minár and Mičian, 2002, adapted). **b**) and **c**) Digital geomorphological maps – expert-based classification of 86 automatically detected elementary forms based on physical-geomorphometric analysis and field verification: (**b**) Initial (on natural) forms; (**c**) Anthropic forms and anthropization of natural forms. Specific elementary forms (segments) are numbered and referred to in the text.

is the best-preserved planation surface truncating inclined Mesozoic limestone. Small boundary segments are characterized by various deformations: 26 – small gravity subsidence, 28 – small structural step, 29 – eroded convex (ridge), and 30 – eroded concave (dell) remnant. Segments 22, 24, and 25 are remnants of the natural planation surface, extended by mining inwards to the fault slope and covered by colluvium from the quarry scarps. They differ in the character of their colluvium: sand in 25, inactive sandstone blocks in 24, and still active rock fall under the main scarp in 22.

The narrow belt of planation north of Sandberg is almost completely covered by the ancient fortification: ramparts and their inner slopes (segments 32–36, 38), inter-rampart depression (31), subsequent anthropo-terrace along the path (37) and related erosional depression (39). They are again characterized by more extreme curvature energies and indexes and lower affinity to an ideal elementary form. Segments 40 and 41 represent the biggest and best-preserved rampart on the rim of the exhumed abrasion surface of Slovinec hill, sharing characteristic signs of previous anthropogenic forms. Segments 42 and 43 are built by resistant Mesozoic limestone exhumed from below Miocene sands. They differ significantly in affinity to z = constant, as in all geomorphic energies. The higher anthropic modification of 43 (remnants of small ramparts, ruins, and waterworks, not distinguished in this segmentation) can be one reason: a change in rock resistance (more and less resistant limestone) can be a second. Slope segment 44 dividing segments 42 and 43 can be a signal of the rock change. The biggest segment of the whole territory (45) represents a relatively subsided part of the cryopediment, in the Vienna Basin. It is formed on soft Miocene sediments as an erosional glacis that merges downward into old Pleistocene river terraces. Indistinct anthropogenic (building) terraces on its south boundary are nearly completely smoothed by the DEM generalization; hence a generally high affinity to z = constant and minimization of all geomorphic energies point to the stationary state of the segment.

That is not the case of the contrast slope (segments 46–57) separating segment 45 from the rest of the cryopediment in the Carpathians. This younger fault-landslide slope formed since the Early-Middle Pleistocene boundary, during the last (late Quaternary) tectonic pulse separating the Carpathians from the Vienna Basin (Bella et al., 2022). Segment 47 was classified as an elementary form with low affinity to z = constant, but its higher $\Delta PES_{(\tau_g)_c}$ and *IPESC* also points to a transition towards the fault slope. It can be identified with the 'tectonically inclined' cryopediment of Minár and Mičian (2002) and classified as a part of that cryopediment. However, we interpret it as a footslope component of the fault-landslide slope, fully represented by segment 46. The remaining segments of the slope consist of embedded anthropic forms: ancient ramparts (54, 56) and their outer slopes (55, 57), an inter-rampart depression (52) that was partially reformed into a modern building terrace (53) together with a part of a rampart (51) and rampart outer slope (50). The slope (48) of the most distinct building terrace (49) is probably remodelled lowermost gravity-tectonic scarp.

The transition between relatively uplifted cryopediment (exhumed abrasion surface) and subsided cryopediment is yet more complicated on the north side of Slovinec hill. Segments 58–60 were classified by Minár and Mičian (2002) as a denudational slope on the lithological boundaries because the slope generally does not follow a straight tectonic line, but rather the circular lithological contact of Mesozoic Limestone and Miocene sand and sandstone. The main segment (59) shows the greatest (but low) affinity to horizontality: it consists of big flat surfaces (blocks) separated by steep short slopes (reflected only in more detailed segmentation). Their origin could be natural (landslide, structural steps) or anthropic (building terraces). Although both factors could play a role, high gravity discordance (Fig. 7 e, h) could point to a dominant role of anthropic modification. This is also the case for segment 58, where the main natural scarp was emphasized by ancient fortification creating the outer slope of the biggest rampart, erosionally degraded in segment 60.

The western slope below the cryopediment (segments 61–79) generally follows a master fault controlling the orientation of the Morava River, which cuts the foothill of the slope. The northern part of the resulting fault-erosion-landslide slope is built of Mesozoic limestone. Its huge rocky erosion scarp has been transformed into an industrial quarry (66) separating small segments (65, 67) of the natural slope. The steep foothill of the quarry scarp is covered by rocky blocks (68), with its gentle part covered by finer colluvium (69). The relatively preserved more moderately-sloping part of the fault-erosion slope (62, 64) is divided by a block landslide (61) and asymmetric gully slope (63) reflecting probably the westernmost fault limit of the Carpathians from the N. A denudational slope developed on the lithological boundary between Mesozoic limestone and Miocene sand. Within it, the segmentation separated a limestone ridge (72) and the asymmetric slope of a big dell (71). Segment 70 represents a bite of the dell into the Early Pleistocene cryopediment. The SW part of the fault-erosion-landslide slope is developed on Miocene sands with occasional thin sandstone layers. It is affected more by block landsliding than by river erosion. The best-preserved segment (76) is surrounded by anthropically remodelled segments. A deep abandoned sand pit to the south consists of an undulating floor (80) and quarry scarps that are more (77, 79) or less (78) well preserved. Originally the largest scarp was the most denuded and backward erosion shifted its rim deep into the cryopediment. The segmentation merged relatively contrasting parts into segment 78, with an exceptional PES_e value (Fig. 7 d) indicating continuing mass flow disequilibrium. Segments 73 and 74 represent the distinct slope and step of an abandoned anthropic terrace. Its less clear continuation can be observed also inside segment 75 which generally came from gravity-tectonic deformation of the upper cryopediment.

The lowermost segments (81–86) represent variously transformed fluvial accumulation forms. The basis of segment 82 is the Middle Pleistocene terrace of the Morava River which is covered by sandy colluvium. Segment 81 is an unstable rim of the terrace on the contact with the sand pit; segment 83 is a remnant of the terrace covered by a talus cone from the upper dell. The Morava River has a two-level floodplain (segments 84–86) here. The upper level (segment 84) is marked by human activity – mining, building, and road construction. The latter emphasizes the natural step (segment 85) between upper and lower floodplain levels. The natural character of the lower floodplain level (segment 86) underlines the minimization of all geomorphic energies (Fig. 7).

4. Summary and conclusion

Physical geomorphometry is based on the coupled study of landform geometry (geometric fields) and physical fields (e.g. Krcho, 1973; Shary et al., 2005; Krcho and Benová, 2013; Florinsky, 2017; Franklin, 2020); it also includes the use of other physical concepts and various physical analogies. It has significant explanatory potential in geomorphology and other geosciences: it can extend their theoretical and methodological basis and facilitate successful applications. Land surface segmentation and digital geomorphological mapping are one such application.

The *geomorphometric representation of geomorphic energy* is a basis for physically-based land surface segmentation. Geomorphic units of various hierarchical levels (land systems, compounded forms, and elementary forms) can be characterized by global (*GGE*), regional (*RGE*), and local (*LGE*) geomorphic energy (eqs. (1), (2), (3)). *LGE* is coupled with the geometry of elementary forms. Parts of the *LGE* applicable for various geomorphic processes are reflected in the local point-based geomorphometric variables (eqs. (4), (5), (6), (17)). The mathematical and physical interrelationships of these variables can be used efficiently in the design of segmentation procedures. The basic physical meanings of elevation a.s.l. (potential gravity energy), slope gradient (downslope gravity force), plan curvature (concentration of flow), and profile curvature (acceleration of flow) have long been known. However, every change of the energy per unit distance also expresses part of the energy: hence elevation derivatives also represent parts of the potential gravity energy.

Minár et al. (2020) defined the energy applicable to mass flow (*PES*) using the sine of slope, and by the normal slope line (profile), normal contour (tangential), and difference curvatures they defined the parts of *PES* changes responsible for acceleration ($\Delta PES_{(k_n)_s}$) and concentration ($\Delta PES_{(k_n)_c}$), plus the summary *PES* excess (PES_e). Here we extend this concept to the energetic interpretation of three other curvatures: basic twisting curvature defining the gravity-discordant change of *PES* ($\Delta PES_{(\tau_g)_c}$), mean curvature defining the potential gravity energy applicable to diffusion (*PESD*), and Casorati curvature defining the Integral Potential Energy of Surface Curvature (*IPESC*). Such unified energetic expression of local point-based geomorphometric variables enables their direct energetic comparison (by summation, difference and ratio) which is crucial for the delimitation and interpretation of elementary forms. It relates also to third-order variables (changes of curvature), which were suggested for elementary land surface segmentation some time ago (Minár, 1992; Minár and Evans, 2008). The innovative evaluation of segment affinity to various ideal types of equilibrium elementary forms (eqs. (21)–(24)) is one of the advantages of this unified energetic expression.

Minimization, dispersal, and variation of geomorphic energy determine various types of equilibrium and instability of elementary forms, reflecting convergence, intermittency, and divergence in land surface development. The energetic state of an elementary form is also linked to the kind of geomorphometric homogeneity (Fig. 4). It can be used to upgrade the Minár and Evans (2008) concept of elementary forms (Fig. 5). Use of the sine of slope (eq. (4)), of tangential and profile curvature (normal curvatures – eqs. (5), (6)) and of the related changes of the normal curvatures (contour line change of tangential, and slope line changes of tangential and profile curvatures) gives the potential for

more exact energetical interpretation. Incorporating twisting curvature (eq. (9)) improves the distinction of gravity concordant and gravity-discordant forms.

Local point-based geomorphometric variables suggested originally as input to elementary land surface segmentation (Minár and Evans, 2008) have similar but not identical physical meanings as those suggested here. Generally, they express only apparent energies, projected into map view (eqs. (4b), (17b)). Curvatures used herein are the basic trio of the curvatures system of Minár et al. (2020), thus they carry complete information about land surface curvature. The combined curvatures (difference curvature – eq. (7), mean curvature – eq. (17), and Casorati curvature – eq. (18)), with strong energetic meanings, are possible alternative inputs to a segmentation procedure. Some authors already evaluated mean curvature and found it useful (e.g. Wieczorek and Migoń, 2014). In our experiments, the incorporation of combined curvatures appeared redundant, probably because the basic trio already covered their information potential. However, we capitalized on the energetic meaning of the combined curvatures in the subsequent geomorphological analysis (Fig. 7).

Some local area-based and regional geomorphometric variables used in segmentation procedures also have an energetic meaning. Regional variables such as elevation above the base of erosion (z_{rel}), distance to nearest stream (d_s), and Stream Power Index (*SPI*) define regional geomorphic energy (eqs. (2), (11), (12), (13)). Index of Connectivity (*IC*) can be considered as logarithmic sum of upstream regional convergence energy ΔPES_a and downstream $\overline{PES}$; connectivity shows natural dependence on both these energies. All these variables, however, determine and reflect the formation of land systems (typological units), rather than elementary forms (Fig. 3). Area-based local variables such as relief (Δz), Topographic Position Index (*TPI*), and openness approximate some regional energy if the window size approaches topographic grain; if they are computed at 1 m window size, they can approximate some local energy. This explains the relative fruitfulness of these variables in various segmentation procedures. However, physical-geomorphometric aspects of local area-based and regional variables are only selectively outlined here and deserve a full separate study. Topics such as quantifications of downslope controls on local drainage (Hjerdt et al., 2004) and sediment flow connectivity expressed by *IC* (Borselli et al., 2008) should be analysed systematically therein.

Generalization of input DEM to the level most suitable for the detection of elementary forms should precede segmentation (Feciskanin and Minár, 2021; Popov et al., 2021). It can be done explicitly – by changing the DEM resolution (e.g. Florinsky and Kuryakova, 2000; Hengl, 2006) or implicitly, by changing the computational window size of derived geomorphometric variables (e.g. Drăguţ et al., 2009). A combination of both approaches was used in this study and led to plausible results. Because the determination of analytical rules to establish an optimal DEM generalization level is problematic, an empirical approach is suggested. Generally, approaches maximizing the information content of the generalized DEM (Hengl, 2006) can be recommended.

Various machine learning procedures and GEOBIA dominate in the recent discourse of land surface segmentation or classification. The advantage of the first is an ability to elaborate complex information and big datasets, well simulating the holistic approach of mapping geomorphologists. The supervised approaches are useful mainly for the identification of specific well-known genetic landforms (e.g. Xiong et al., 2022 and citations therein). Wall-to-wall physically-based elementary segmentation, however, should be more heuristic – looking for the specific physical-geomorphic spatial structures that can subsequently be genetically (or dynamically) interpreted. In principle, the segmentation requires the unsupervised approach, but the key role is not the procedure itself, but its input variables and the ability of the procedure to respect the described mathematical-physical relationships.

GEOBIA is a suitable tool for physically-based elementary land surface segmentation, providing for energetic homogeneity of the resultant objects. The geometric values of local point-based variables directly reflect their energetic meaning. Energetically, elevation > slope > curvatures > changes of curvature. Hence the emphasis on horizontal planes (z = const.) and linear facets (S, A = const.) in traditional geomorphological mapping has an energetic explanation: their formation requires the biggest energetic input, and so they are the most distinct morphogenetic equilibrium individuals. The mathematical interrelationship of local point-based variables provides for the preferred identification of plain and linear segments, disregarding the number of input curvatures and changes of curvatures. An ideal horizontal plane has homogenous (zero) values of all derived local point variables; an ideal linear slope has all curvatures and changes of curvatures homogeneous (at zero). Therefore increasing the number of inputs (curvatures and changes of curvatures) does not attenuate but reinforces the identification of plains and linear facets. The DEM surfaces depart, however, from the ideal because of inherent errors during data acquisition, as well as the persistent issue of the calibration to scale. Making the concept of minimization of geomorphic energy in elementary forms operational thus requires managing the appropriate tolerance around zero values (i.e. making operational the concept of homogeneity) relative to the DEM at hand. Object-oriented analysis can handle this issue, as it has the built-in concept of homogeneity in the definition of objects from raster data. Moreover, the appropriate degree of homogeneity is determined statistically (by measuring the local variance) with the ESP tool.

Digital geomorphological mapping in a broad sense can be considered as a digital collection of information layers for the modern geomorphological map by using information from DEMs (e.g. Garcia and Grohmann, 2019): its further development, however, consists in the (semi-) automated extraction and classification of geomorphological features from DEMs (Seijmonsbergen, 2013; Li and Zhao, 2022). Moreover, a detailed geomorphological map should also be a synthesis of broad research (De Jong et al., 2021) including geomorphometric, morphodynamic, morphogenetic, morphochronologic, and lithologic data (Minár et al., 2005; Gustavsson et al., 2006). Other than geomorphometry, the detailed spatial distribution of the majority of this information is hidden. Therefore, the spatial distribution of elementary forms with interconnected geometric, physical, and geosystem properties can well reflect not only the spatial distribution of morphogenetic, morphochronologic, morphodynamic, and lithologic properties but also other essential characteristics of the natural landscape: soil, microclimatic and hydrologic regimes and potential vegetation (e.g. Minár, 2003; Barka et al., 2011; Romstad and Etzelmüller, 2012; Mokarram and Sathyamoorthy, 2018; Petrikovičová et al., 2020).

As documented in the worked example (Fig. 8), physically-based elementary land surface segmentation produces resultant segments with clear morphogenetic and morphodynamic interpretations. A geomorphologist can assign morphogenetic individuality to every segment, so the segmentation can be directly used for the construction of a geomorphological map. Traditional qualitative expert-based mapping can be significantly improved (complemented) in this way. The physical-geomorphometric characterization of segments (Fig. 7) is an analytical tool for (expert-based) deduction of genetic and dynamic interpretations. Moreover, it can facilitate the construction and testing of non-trivial scientific hypotheses. Analysing the human topographic signature, Tarolli and Sofia (2016) recognised the diagnostic potential of the 'surface peak curvature' for detecting anthropic forms. Our anthropic forms and anthropized natural forms in Fig. 8c visually correspond well with higher geomorphic energies and instability (Fig. 7) related to the curvatures. Thus, it is possible to test a hypothesis that various kinds of anthropization, and the age, velocity, and type of renaturalization of the abandoned anthropic forms, have specific expressions in geomorphic energies and instability indexes that can be compared with empiric results such as those presented in Tarolli and Sofia (2016).

The morphogenetic information of our results is compatible with the

hierarchical geomorphological mapping of De Jong et al. (2021). The morphogenetic classification of our Fig. 8 corresponds to their 'Tier 2', suggested for scales of 1:10,000–1: 30,000. The following detailed morphogenetic description of particular segments corresponds to their 'Tier 3' (scales 1: 2500–1:10,000). However, the manual delineation of the most detailed Tier 3 objects is substituted in our case by automatic GEOBIA segmentation. Recent attempts to automate wall-to-wall ('full coverage') detailed digital geomorphological mapping typically used segmentation methods based on variables with physical meaning. They are not only local point-based variables as suggested by us (e.g. Gerçek et al., 2011; Foroutan et al., 2013; Mashimbye et al., 2014; Furlan et al., 2018) but also local area-based and regional variables such as z_{rel} (e.g. Gharari et al., 2011), *TPI* (e.g. Trentin and Robaina, 2018; Bufalini et al., 2021; Siervo et al., 2023) or openness – geomorphons (e.g. Dutra et al., 2020; de Amorim et al., 2021). However, the resultant units were interpreted only morphologically or in terms of descriptive statistics. Incorporation of any individual quantitative measures is exceptional (e. g. Hansen et al., 2021). On the contrary, the physically-based approach generates individual geometric, physical and geosystem specifications of each object, extending possibilities of scientific and practical applications. It can be used for morphodynamic analysis (e.g. by Fryirs and Brierley, 2022) and also for morphogenetic interpretation as presented here. The effectiveness of results of geomorphometric research depends not only on measurement and computational quality but also on the exact definition of measured objects and exactness of interpretation of the geomorphometric variables (Minár et al., 2015; Sofia, 2020). Hence physical geomorphometry can contribute to the reproducible character of geosciences.

Declaration of Competing Interest

The authors declare that they have no known competing financial interests or personal relationships that could have appeared to influence the work reported in this paper.

Data availability

Data will be made available on request.

Acknowledgement

This work was supported by the Slovak Research and Development Agency under the contracts No. APVV-15-0054 and APVV-22-0024.

References

Abrahams, A.D., 1968. Distinguishing between the concepts of steady state and dynamic equilibrium in geomorphology. Earth Sci. J. 2 (2), 160–166.

Adediran, A.O., Parcharidis, I., Poscolieri, M., Pavlopoulos, K., 2004. Computer-assisted discrimination of morphological units on northcentral Crete (Greece) by applying multivariate statistics to local relief gradients. Geomorphology 58, 357–370. https://doi.org/10.1016/j.geomorph.2003.07.024.

Alvioli, M., Marchesini, I., Reichenbach, P., Rossi, M., Ardizzone, F., Fiorucci, F., Guzzetti, F., 2016. Automatic delineation of geomorphological slope units with r. slopeunits v1.0 and their optimization for land-slide susceptibility modeling. Geosci. Model Dev. 812 (9), 3975–3991. https://doi.org/10.5194/gmd-9-3975-2016.

Amatulli, G., Domisch, S., Tuanmu, M.N., Parmentier, B., Ranipeta, A., Malczyk, J., Jetz, W., 2018. A suite of global, cross-scale topographic variables for environmental and biodiversity modeling. Sci. Data 5, 180040. https://doi.org/10.1038/sdata.2018.40.

Anders, N.S., Seijmonsbergen, A.C., Bouten, W., 2011. Segmentation optimization and stratified object-based analysis for semi-automated geomorphological mapping. Remote Sens. Environ. 115, 2976–2985. https://doi.org/10.1016/j.rse.2011.05.007.

Anders, N.S., Seijmonsbergen, A.C., Bouten, W., 2015. Rule set transferability for object-based feature extraction: an example for cirque mapping. Photogramm. Eng. Remote. Sens. 81 (6), 507–514. https://doi.org/10.14358/PERS.81.6.507.

Anderson, R.S., 2002. Modeling the tor-dotted crests, bedrock edges, and parabolic profiles of high alpine surfaces of the Wind River Range, Wyoming. Geomorphology 46 (1–2), 35–58. https://doi.org/10.1016/S0169-555X(02)00053-3.

Baatz, M., Schäpe, A., 2000. Multiresolution segmentation: an optimization approach for high quality multi-scale image segmentation. In: Strobl, J., Blaschke, T., Griesbner, G. (Eds.), Angewandte Geographische Informations-Verarbeitung, XII. Wichmann, Karlsruhe, pp. 12–23.

Bandura, P., Minár, J., Bielik, M., 2021. Physically based morphostructural land surface segmentation: Case of the Alps and Western Carpathians. Trans. GIS 25, 2394–2418. https://doi.org/10.1111/tgis.12847.

Barbarella, M., Di Benedetto, A., Fiani, M., 2021. Application of supervised machine learning technique on LiDAR data for monitoring coastal land evolution. Remote Sens. 13 (23), 4782. https://doi.org/10.3390/rs13234782.

Barka, I., Vladovič, J., Máliš, F., 2011. Landform classification and its application in predictive mapping of soil and forest units. In: Proceedings of the GIS Ostrava, Ostrava, Czech Republic, 24–26 January 2011, p. 11.

Bella, P., Hercman, H., Kdýr, Š., Mikysek, P., Pruner, P., Littva, J., Minár, J., Gradziński, M., Wróblewski, W., Velšmid, M., Bosák, P., 2022. Sulfuric acid speleogenesis and surface landform evolution along the Vienna Basin Transfer Fault: Plavecký Karst, Slovakia. Int. J. Speleol. 51 (2), 105–122. https://doi.org/10.5038/1827-806x.51.2.2420.

Beven, K.J., Kirkby, M.J., 1979. A physically based, variable contributing area model of basin hydrology. Hydrol. Sci. J. 24, 43–69. https://doi.org/10.1080/02626667909491834.

Bishop, M.P., James, L.A., Shroder Jr., J.F., Walsh, S.J., 2012. Geospatial technologies and digital geomorphological mapping: concepts, issues and research. Geomorphology 137, 5–26. https://doi.org/10.1016/j.geomorph.2011.06.027.

Blaschke, T., 2010. Object based image analysis for remote sensing. ISPRS J. Photogramm. Remote Sens. 65, 2–16. https://doi.org/10.1016/j.isprsjprs.2009.06.004.

Blaschke, T., Strobl, J., 2003. Defining landscape units through integrated morphometric characteristics. In: Buhman, E., Ervin, S. (Eds.), Landscape Modelling: Digital Techniques for Landscape Architecture. Wichmann, Heidelberg, pp. 104–113.

Bock, A., Leyk, S., 2011. Scale-specific modeling of class-level uncertainty in landform taxonomies using fuzzy sets. In: Hengl, T., Evans, I.S., Wilson, J.P., Gould, M. (Eds.), Proceedings of Geomorphometry 2011. International Society for Geomorphometry, Redlands, California, pp. 133–136.

Bolongaro-Crevenna, A., Torres-Rodríguez, V., Sorani, V., Frame, D., Ortiz, M.A., 2005. Geomorphometric analysis for characterizing landforms in Morelos State Mexico. Geomorphology 67, 407–422. https://doi.org/10.1016/j.geomorph.2004.11.007.

Borselli, L., Cassi, P., Torri, D., 2008. Prolegomena to sediment and flow connectivity in the landscape: a GIS and field numerical assessment. Catena 75, 268–277.

Bufalini, M., Materazzi, M., De Amicis, M., Pambianchi, G., 2021. From traditional to modern "full coverage" geomorphological mapping: a study case in the Chienti river basin (Marche region, Central Italy). J. Maps 17 (3), 17–28. https://doi.org/10.1080/17445647. 2021.1904020.

Cavalli, M., Trevisani, S., Comiti, F., Marchi, L., 2013. Geomorphometric assessment of spatial sediment connectivity in small Alpine catchments. Geomorphology 188, 31–41. https://doi.org/10.1016/j.geomorph.2012.05.007.

Cheng, W., Zhou, C., Chai, H., Zhao, S., Liu, H., Zhou, Z., 2011. Research and compilation of the Geomorphologic Atlas of the People's Republic of China (1: 1,000,000). J. Geogr. Sci. 21 (1), 89–100. https://doi.org/10.1007/s1144 2-011-0831-z.

Chrobak, A., Novotny, J., Strus, P., 2021. Geodiversity assessment as a first step in designating areas of geotourism potential. Case study: Western Carpathians. Front. Earth Sci. 9, 752669 https://doi.org/10.3389/feart.2021.752669.

Clubb, F.J., Mudd, S.M., Milodowski, D.T., Hurst, M.D., Slater, L.J., 2014. Objective extraction of channel heads from high-resolution topographic data. Water Resour. Res. 50, 4283–4304. https://doi.org/10.1002/2013WR015167.

Conoscenti, C., Rotigliano, E., 2020. Predicting gully occurrence at watershed scale: comparing topographic indices and multivariate statistical models. Geomorphology 359, 107123 doi: 10. 1016/j. geomorph.2020. 107123.

Crema, S., Bossi, G., 2017. Clustering sediment connectivity maps to distinguish hillslope processes. Italian Geol. Soc. 42, 23–26.

Csillik, O., Evans, I.S., Drăguţ, L., 2015. Transformation (normalization) of slope gradient and surface curvatures, automated for statistical analyses from DEMs. Geomorphology 232, 65–77. https://doi.org/10.1016/j.geomorph.2014.12.038.

Daggupati, P., Douglas-Mankin, K.R., Sheshukov, A.Y., 2013. Predicting ephemeral gully location and length using topographic index models. Trans. ASABE 56 (4), 1427–1440. https://doi.org/10.13031/trans.56.10087.

de Amorim, L.D.O., de Souza Robaina, L.E., Trentin, R., 2021. Automated analysis of landforms of the Paraguaçu River Basin / Bahia. Rev. Brasil. Geomorfol. 22 (3), 641–655.

De Jong, M.G.G., Sterk, H.P., Shinneman, S., Seijmonsbergen, A.C., 2021. Hierarchical geomorphological mapping in mountainous areas. J. Maps 17 (2), 214–224. https://doi.org/10.1080/17445647.2021.1897047.

Dekavalla, M., Argialas, D., 2017. Evaluation of a spatially adaptive approach for land surface classification from digital elevation models. Int. J. Geogr. Inf. Sci. 31 (10), 1978–2000. https://doi.org/10.1080/13658816.2017.1344984.

Devlin, J.F., 2003. Rationalizing geomorphology with an energy balance. J. Geosci. Educ. 51, 398–409. https://doi.org/10.5408/1089-9995-51.4.398.

Dikau, R., 1989. The application of a digital relief model to landform analysis in geomorphology. In: Raper, J. (Ed.), Three-Dimensional Applications in Geographical Information Systems. Taylor & Francis, London, pp. 51–77.

Ding, H., Na, J., Jiang, S., Zhu, J., Liu, K., Fu, Y., Li, F., 2021. Evaluation of three different machine learning methods for object-based artificial terrace mapping—a case study of the loess plateau. China. Remote Sens. 13 (5), 1021. https://doi.org/10.3390/rs13051021.

d'Oleire-Oltmanns, S., Eisank, C., Drägut, L., Blaschke, T., 2013. An object-based workflow to extract landforms at multiple scales from two distinct data types. IEEE Geosci. Remote Sens. Lett. 10 (4), 947–951. https://doi.org/10.1109/LGRS.2013.2254465.

Drăguţ, L., Blaschke, T., 2006. Automated classification of landform elements using object-based image analysis. Geomorphology 81 (3–4), 330–344. https://doi.org/10.1016/j.geomorph.2006.04.013.
Drăgut, L., Blaschke, T., 2008. Terrain segmentation and classification using SRTM data. In: Zhou, Q., Lees, B., Tang, G.-A. (Eds.), Advances in Digital Terrain Analysis. Springer, Berlin, pp. 141–158.
Drăguţ, L., Schauppenlehner, T., Muhar, A., Strobl, J., Blaschke, T., 2009. Optimization of scale and parametrization for terrain segmentation: an application to soil-landscape modeling. Comput. Geosci. 35 (9), 1875–1883. https://doi.org/10.1016/j.cageo.2008.10.008.
Drăguţ, L., Tiede, D., Levick, S.R., 2010. ESP: a tool to estimate scale parameter for multiresolution image segmentation of remotely sensed data. Int. J. Geogr. Inf. Sci. 24 (6), 859–871. https://doi.org/10.1080/13658810903174803.
Drăguţ, L., Minár, J., Csillik, O., Evans, I.S., 2013. Land-surface segmentation to delineate elementary forms from Digital Elevation Models. In: Geomorphometry 2013 Conference Proceedings. Nanjing Normal University, China, pp. 42–45. http://geomorphometry.org/Dragut2013.
Drăguţ, L., Csillik, O., Eisank, C., Tiede, D., 2014. Automated parameterisation for multi-scale image segmentation on multiple layers. ISPRS J. Photogramm. Remote Sens. 88, 119–127. https://doi.org/10.1016/j.isprsjprs.2013.11.018.
Dramis, F., Guida, D., Cestari, A., 2011. Nature and aims of geomorphological mapping. In: Smith, M.J., Paron, P., Griffiths, J.S. (Eds.), Developments in Earth Surface Processes: Geomorphological Mapping. Elsevier, Amsterdam, pp. 39–73. https://doi.org/10.1016/B978-0-444-53446-0.00003-3.
Dutra, D.D.S., Furlan, A.R., Robaina, L.E.S., 2020. Subdivision of relief elements through the proposal of geomorphons: river basin of arroio Pantanoso – Canguçu/RS. Rev. Brasil. Geografia Fisica 13 (2), 713–726.
Ehsani, A.H., Quiel, F., 2008. Geomorphometric feature analysis using morphometric parameterization and artificial neural networks. Geomorphology 99 (1–4), 1–12. https://doi.org/10.1016/j.geomorph.2007.10.002.
Evans, I.S., 1972. General geomorphometry, derivatives of altitude and descriptive statistics. In: Chorley, R.J. (Ed.), Spatial Analysis in Geomorphology. Methuen, London, pp. 17–90.
Evans, I.S., 2003. Scale-specific landforms and aspects of the land surface. In: Evans, I.S., Dikau, R., Tokunaga, E., Ohmori, H., Hirano, M. (Eds.), Concepts and Modelling in Geomorphology: International Perspectives. Terrapub, Tokyo, pp. 61–84.
Evans, I.S., 2012. Geomorphometry and landform mapping: what is a landform? Geomorphology 137 (1), 94–106. https://doi.org/10.1016/j.geomorph.2010.09.029.
Evans, I.S., Minár, J., 2011. A classification of geomorphometric variables. In: Hengl, T., Evans, I.S., Wilson, J.P., Gould, M. (Eds.), Proceedings of Geomorphometry 2011. International Society for Geomorphometry, Redlands, California, pp. 105–108.
Feciskanin, R., Minár, J., 2021. Polygonal simplification and its use in DEM generalization for land surface segmentation. Trans. GIS 25 (5), 2361–2375. https://doi.org/10.1111/tgis.12796.
Feizizadeh, B., Kazamei, M., Blaschke, T., Lakes, T., 2021. An object-based image analysis applied for volcanic and glacial landforms mapping in Sahand Mountain, Iran. Catena 198, 105073. https://doi.org/10.1016/j.catena.2020.105073.
Florinsky, I.V., 1998. Accuracy of local topographic variables derived from digital elevation models. Int. J. Geogr. Inf. Sci. 12 (1), 47–62. https://doi.org/10.1080/136588198242003.
Florinsky, I.V., 2009. Computation of the third-order partial derivatives and derivation function from a digital elevation model. Int. J. Geogr. Inf. Sci. 23 (2), 213–231. https://doi.org/10.1080/13658810802527499.
Florinsky, I.V., 2017. An illustrated introduction to general geomorphometry. Progr. Phys. Geogr.–Earth Environ. 41 (6), 723–752. https://doi.org/10.1177/0309133317733667.
Florinsky, I.V., 2018. Multiscale geomorphometric modeling of Mercury. Planet. Space Sci. 151 (2018), 56–70. https://doi.org/10.1016/j.pss.2017.11.010.
Florinsky, I.V., Kuryakova, G.A., 2000. Determination of grid size for digital terrain modelling in landscape investigations—exemplified by soil moisture distribution at a micro-scale. Int. J. Geogr. Inf. Sci. 148, 815–832. https://doi.org/10.1080/136588100750022804.
Foroutan, M., Kompanizare, M., Ehsani, A.H., 2013. Semiautomatic morphometric land surface segmentation of an arid mountainous area using DEM and self-organizing maps. Arab. J. Geosci. 6 (12), 4795–4810. https://doi.org/10.1007/s12517-012-0797-x.
Franklin, S.E., 2020. Interpretation and use of geomorphometry in remote sensing: a guide and review of integrated applications. Int. J. Remote Sens. 41 (19), 7700–7733. https://doi.org/10.1080/01431161.2020.1792577.
Fryirs, K., Brierley, G., 2022. Assemblages of geomorphic units: a building block approach to analysis and interpretation of river character, behaviour, condition and recovery. Earth Surf. Process. Landf. 47 (1), 92–108. https://doi.org/10.1002/esp.5264.
Furlan, A.R., Dias, D.F., Trentin, R., Robaina, L.E.S., 2018. Identificação das unidades geomorfométricas da bacia hidrográfica do arroio Carijinho, Rio Grande do Sul, Brasil. Rev. Brasil. Geomorfol. 19, 807–820, 10.20502/rbg.v19i4.1377.
Gallant, J.C., Hutchinson, M.F., 2011. A differential equation for specific catchment area. Water Resour. Res. 47 (5) https://doi.org/10.1029/2009WR008540.
Gallant, J.C., Wilson, J.P., 2000. Primary topographic attributes. In: Wilson, J.P., Gallant, J. (Eds.), Terrain Analysis: Principles and Applications. Wiley, New York, pp. 51–85.
Garajeh, K.M., Feizizadeh, B., Weng, Q., Rezaei Moghaddam, M.H., Kazemi Garajeh, A., 2022. Desert landform detection and mapping using a semi-automated object-based image analysis approach. J. Arid Environ. 199, 104721 https://doi.org/10.1016/j.jaridenv.2022.104721.
Garcia, G.P.B., Grohmann, C.H., 2019. DEM-based geomorphological mapping and landforms characterization of a tropical karst environment in southeastern Brazil. J. S. Am. Earth Sci. 93, 14–22. https://doi.org/10.1016/j.jsames.2019.04.013.
Garland, M., Heckbert, P.S., 1997. Surface simplification using quadric error metrics. In: Proceedings of the 24th Annual Conference on Computer Graphics and Interactive Techniques. Los Angeles, CA, pp. 209–216.
Gauss, C.F., 1828. Disquisitiones generales circa superficies curvas. Gott. Gel. Anz. No 177, 1761–1768 (in Latin).
Gerçek, D., Toprak, V., Strobl, J., 2011. Object-based classification of landforms based on their local geometry and geomorphometric context. Int. J. Geogr. Inf. Sci. 25 (6), 1011–1023. https://doi.org/10.1080/13658816.2011.558845.
Gharari, S., Hrachowitz, M., Fenicia, F., Savenije, H.H.G., 2011. Hydrological landscape classification: investigating the performance of HAND based landscape classifications in a central European meso-scale catchment. Hydrol. Earth Syst. Sci. 15, 3275–3291. https://doi.org/10.5194/hess-15-3275-2011.
Giaccone, E., Oriani, F., Tonini, M., Lambiel, C., Mariéthoz, G., 2022. Using data-driven algorithms for semi-automated geomorphological mapping. Stoch. Env. Res. Risk Assess. 36, 2115–2131. https://doi.org/10.1007/s00477-021-02062-5.
Gilbert, G.K., 1909. The convexity of hilltops. J. Geol. 17 (4), 344–350.
Giles, P.T., 1998. Geomorphological signatures: Classification of aggregated slope unit objects from digital elevation and remote sensing data. Earth Surf. Process. Landf. 23 (7), 581–594. https://doi.org/10.1002/(SICI)1096-9837(199807)23:7<581::AID-ESP863>3.0.CO;2-S.
Glock, W.S., 1932. Available relief as a factor of control in the profile of a landform. J. Geol. 40 (1), 74–83.
González-Díez, A., Barreda-Argüeso, J.A., Rodríguez-Rodríguez, L., Fernández-Lozano, J., 2021. The use of filters based on the Fast Fourier Transform applied to DEMs for the objective mapping of karstic features. Geomorphology 385, 107724. https://doi.org/10.1016/j.geomorph.2021.107724.
Gonzalez-Hidalgo, J.C., Batalla, R.J., Cerda, A., 2012. Catchment size and contribution of the largest daily events to suspended sediment load on a continental scale. Catena 102, 40–45. https://doi.org/10.1016/j.catena.2010.10.011.
Gray, M., 2019. Geodiversity, geoheritage and geoconservation for society. Int. J. Geoheritage Parks 7, 226–236. https://doi.org/10.1016/j.ijgeop.2019.11.001.
Guida, D., Cuomo, A., Palmieri, V., 2016. Using object-based geomorphometry for hydro-geomorphological analysis in a Mediterranean research catchment. Hydrol. Earth Syst. Sci. 20, 3493–3509. https://doi.org/10.5194/hess-20-3493-2016.
Guilbert, E., Moulin, B., 2017. Towards a common framework for the identification of landforms on terrain models. ISPRS Int. J. Geo-Information 6 (1), 12. https://doi.org/10.3390/ijgi6010012.
Gustavsson, M., Kolstrup, E., Seijmonsbergen, A.C., 2006. A new symbol-and-GIS based detailed geomorphological mapping system: Renewal of a scientific discipline for understanding landscape development. Geomorphology 77 (1–2), 90–111. https://doi.org/10.1016/j.geomorph.2006.01.026.
Hansen, L.Ø., Ernstsen, V.B., Clemmensen, L.B., Al-Hamdani, Z., Kroon, A., 2021. A method for estimating sediment budgets of washover deposits using digital terrain models. Earth Surf. Process. Landf. 46, 804–821. https://doi.org/10.1002/esp.5066.
Heckmann, T., et al., 2018. Indices of sediment connectivity: opportunities, challenges and limitations. Earth Sci. Rev. 187, 77–108.
Hengl, T., 2006. Finding the right pixel size. Comput. Geosci. 32 (9), 1283–1298. https://doi.org/10.1016/j.cageo.2005.11.008.
Hjerdt, K.N., McDonnell, J.J., Seibert, J., Rodhe, A., 2004. A new topographic index to quantify downslope controls on local drainage. Water Resour. Res. 40, W05602. https://doi.org/10.1029/2004WR003130.
Huggett, R.J., 2007. A history of the systems approach in geomorphology. Géomorphol. Relief, Proc. Environ. 13 (2), 145–158. https://doi.org/10.4000/geomorphologie.1031.
Hurst, M.D., Mudd, S.M., Walcott, R., Attal, M., Yoo, K., 2012. Using hilltop curvature to derive the spatial distribution of erosion rates. J. Geophys. Res. 117, 1–19. https://doi.org/10.1029/2011JF002057.
Ilinca, V., 2021. Using morphometrics to distinguish between debris flow, debris flood and flood (Southern Carpathians, Romania). Catena 197, 104982. https://doi.org/10.1016/j.catena.2020.104982.
Irvin, B.J., Ventura, S.J., Slater, B.K., 1997. Fuzzy and isodata classification of landform elements from digital terrain data in Pleasant Valley, Wisconsin. Geoderma 77, 137–154.
Iwahashi, J., Yamazaki, D., Nakano, T., Endo, R., 2021. Classification of topography for ground vulnerability assessment of alluvial plains and mountains of Japan using 30 m DEM. Prog. Earth Planet Sci. 8, 3. https://doi.org/10.1186/s40645-020-00398-0.
Jasiewicz, J., Stepinski, T.F., 2013. Geomorphons – a pattern recognition approach to classification and mapping of landforms. Geomorphology 182, 147–156. https://doi.org/10.1016/j.geomorph.2012.11.005.
Jenčo, M., 1992. The morphometric analysis of georelief in terms of a theoretical conception of the complex digital model of georelief. Acta Facultatis Rerum Naturalium Universitatis Comenianae, Geographica 33, 133–153.
Jenčo, M., 2018. Detection of degenerate points on the surface. PeerJ Preprints 6, e27097v1. https://doi.org/10.7287/peerj.preprints.27097v1.
Józsa, E., Fábián, S.A., 2016. Mapping landforms and geomorphological landscapes of Hungary using GIS techniques. Stud. Geomorphol. Carpatho-Balcanica 50, 19–31.
Kazhdan, M., Bolitho, M., Hoppe, H., 2006. Poisson surface reconstruction. In: Proceedings of the Fourth Eurographics Symposium on Geometry processing, 2006, p. 10.
Kirkby, M.J., 1996. A role for theoretical models in geomorphology? In: Rhoads, B.L., Thorn, C.E. (Eds.), The Scientific Nature of Geomorphology: Proceedings of the 27th Binghamton Symposium in Geomorphology. Wiley, pp. 257–272.

Koenderink, J.J., van Doorn, A.J., Wagemans, J., 2015. Local solid shape. i-Perception 6 (5), 2041669515604063. https://doi.org/10.1177/2041669515604063.
Krcho, J., 1973. Morphometric analysis of relief on the basis of geometric aspect of field theory. Acta Geographica Universit. Comenianae, Geographico–physica No. 1, 7–233.
Krcho, J., 1979. Reliéf ako priestorový subsystem SRF geografickej krajiny a jeho komplexný digitálny model (KDMT)., [Relief as the spatial subsystem SRF of geographical landscape and its Complex Digital Model (CDTM)]. Geografický časopis 31 (3), 237–262 (in Slovak).
Krcho, J., 1983. Teoretická koncepcia a interdisciplinárne aplikácie komplexného digitálneho modelu reliéfu pri modelovaní dvojdimenzionálnych polí., [Theoretical conception and interdisciplinary applications of the complex digital model of relief in modeling bidimensional fields]. Geografický časopis 35 (3), 265–291 (in Slovak).
Krcho, J., Benová, A., 2013. Problém správnej a exaktnej definície geometrických foriem georeliéfu vzhľadom na tiažové pole Zeme., [The problem of correct and exact definition of geometrical forms of georelief regarding the Earth's gravitational field]. Geografický časopis 65 (3), 189–216 (in Slovak).
Li, S., Xiong, L., Tang, G., Strobl, J., 2020. Deep learning-based approach for landform classification from integrated data sources of digital elevation model and imagery. Geomorphology 354, 107045. https://doi.org/10.1016/j.geomorph.2020.107045.
Lastochkin, A.N., Zhirov, A.I., Boltramovich, S.F., 2018. System-morphological approach: another look at morphology research and geomorphological mapping. Geomorphology 303, 486–503. https://doi.org/10.1016/j.geomorph.2017.10.022.
Li, W., Hsu, C.-Y., Hu, M., 2021. Tobler's First Law in GeoAI: a spatially explicit deep learning model for terrain feature detection under weak supervision. Ann. Am. Assoc. Geogr. 111 (7), 1887–1905. https://doi.org/10.1080/24694452.2021.1877527.
Li, Y., Zhao, Z., 2022. AutoCirque: an automated method to delineate glacial cirque outlines from digital elevation models. Geomorphology 398, 108059. https://doi.org/10.1016/j.geomorph.2021.108059.
Lindsay, J.B., Cockburn, J.M.H., Russell, H.A.J., 2015. An integral image approach to performing multi-scale topographic position analysis. Geomorphology 245, 51–61. https://doi.org/10.1016/j.geomorph.2015.05.025.
Lindsay, J.B., Francioni, A., Cockburn, J.M.H., 2019. LiDAR DEM smoothing and the preservation of drainage features. Remote Sens. 11 (16), 1926. https://doi.org/10.3390/rs11161926.
Lisenby, P.E., Croke, J., Fryirs, K.A., 2018. Geomorphic effectiveness: a linear concept in a non-linear world. Earth Surf. Process. Landf. 43, 4–20. https://doi.org/10.1002/esp.4096.
Louw, G., van Niekerk, A., 2019. Object-based land surface segmentation scale optimisation: an ill-structured problem. Geomorphology 327, 377–384. https://doi.org/10.1016/j.geomo rph.2018.11.021.
Lundblad, E.R., Wright, D.J., Miller, J., Larkin, E.M., Rinehart, R., Naar, D.F., Donahue, B.T., Anderson, S.M., Battista, T., 2006. A benthic terrain classification scheme for American Samoa. Mar. Geod. 29, 89–111.
MacMillan, R.A., Shary, P.A., 2009. Landforms and landform elements in geomorphometry. In: Hengl, T., Reuter, H.I. (Eds.), Geomorphometry: Concepts, Software, Applications. Developments in Soil Science, 33. Elsevier, pp. 227–254. https://doi.org/10.1016/S0166-2481(08)00009-3. Geomorphometry.
MacMillan, R.A., Pettapiece, W.W., Nolan, S.C., Goddard, T.W., 2000. A generic procedure for automatically segmenting landforms into landform elements using DEMs, heuristic rules and fuzzy logic. Fuzzy Sets Syst. 113, 81–109. https://doi.org/10.1016/S0165-0114(99)00014-7.
Marchi, L., Dalla Fontana, G., 2005. GIS morphometric indicators for the analysis of sediment dynamics in mountain basins. Environ. Geol. 48, 218–228. https://doi.org/10.1007/s00254-005-1292-4.
Martin, Y., Church, M., 1997. Diffusion in landscape development models: on the nature of basic transport relations. Earth Surf. Process. Landf. 22, 273–279. https://doi.org/10.1002/(SICI)1096-9837(199703)22:3<273::AID-ESP755>3.0.CO;2-D.
Mashimbye, Z., de Clerq, W., van Niekerk, A., 2014. An evaluation of digital elevation models (DEMs) for delineating land components. Geoderma 213, 312–319. https://doi.org/10.1016/j.geoderma.2013.08.023.
Maxwell, A.E., Shobe, C.M., 2022. Land-surface parameters for spatial predictive mapping and modeling. Earth Sci. Rev. 226, 103944 https://doi.org/10.1016/j.earscirev.2022.103944.
McKean, J., Roering, J., 2004. Objective landslide detection and surface morphology mapping using high-resolution airborne laser altimetry. Geomorphology 57, 331–351. https://doi.org/10.1016/S0169-555X(03)00164-8.
Meijles, E.W., Marcos, D.L., Harkema, T.T., Candel, J.H., Maas, G.J., 2022. Comparing geomorphological maps made manually and by deep learning. Earth Surf. Process. Landf. 47 (4), 1089–1107. https://doi.org/10.1002/esp.5305.
Melton, M.A., 1965. The geomorphic and paleoclimatic significance of alluvial deposits in Southern Arizona. J. Geol. 73, 1–38.
Mentlík, P., Novotná, M., 2010. Elementary forms and 'scientific reliability' as an innovative approach to geomorphological mapping. J. Maps 6 (1), 564–583. https://doi.org/10.4113/jom.2010.1144.
Mentlík, P., Jedlička, K., Minár, J., Barka, I., 2006. Geomorphological information system: physical model and options of geomorphological analysis. Geografie 111, 15–32.
Minár, J., 1992. The principles of the elementary geomorphological regionalization. Acta Facultatis Rerum Naturalium Universitatis Comenianae. Geographica 33, 185–198.
Minár, J., 2003. Detailed physical-geographical (geoecological) research and mapping in the landscape ecology. Ekol. Bratisl. 22 (Suppl. 2), 141–149.
Minár, J., Evans, I.S., 2008. Elementary forms for land surface segmentation: the theoretical basis of terrain analysis and geomorphological mapping. Geomorphology 95, 236–259. https://doi.org/10.1016/j.geomorph.2007.06.003.
Minár, J., Mičian, Ľ., 2002. Complex geomorphological characteristics of the Devínska Kobyla Mt. In: Landscape Atlas of the Slovak Republic. Ministry of Environment of the Slovak Republic, Bratislava. Slovak Environmental Agency, Banská Bystrica, pp. 92–93.
Minár, J., Bizubová, M., Machová, Z., Barka, I., 2003. Sandberg (Malé Karpaty Mts.) – the Quaternary tectonics and its consequences. Geomorphol. Slovaca 3 (1), 97–100.
Minár, J., Bizubová, M., Gallay, M., 2004. General aspects of denudation chronology of the West Carpathians. Stud. Geomorphol. Carpatho-Balcanica 38, 5–22.
Minár, J., Mentlík, P., Jedlička, K., Barka, I., 2005. Geomorphological information system — idea and options of practical implementation. Geografický časopis 58, 247–266.
Minár, J., Evans, I.S., Krcho, J., 2013a. Geomorphometry: Quantitative land-surface analysis. In: Shroder, J.F. (Ed.), Treatise on Geomorphology, vol. 14. Academic Press, San Diego, pp. 22–34.
Minár, J., Jenčo, M., Evans, I.S., Minár Jr., J., Kadlec, M., Krcho, J., Pacina, J., Burian, L., Benová, A., 2013b. Third-order geomorphometric variables (derivatives): definition, computation and utilization of changes of curvatures. Int. J. Geogr. Inf. Sci. 27 (7), 1381–1402. https://doi.org/10.1080/13658816.2013.792113.
Minár, J., Minár Jr., J., Evans, I.S., 2015. Towards exactness in geomorphometry. In: Jasiewicz, J., Zwoliński, Z., Mitasova, H., Hengl, T. (Eds.), Geomorphometry for Geosciences. Bogucki Wydawnictwo Naukowe, Poznan, pp. 27–30.
Minár, J., Bandura, P., Holec, J., Popov, A., Gallay, M., Hofierka, J., Kaňuk, J., Drăguţ, L., Evans, I.S., 2018. Physically-based land surface segmentation: Theoretical background and outline of interpretations. PeerJ Preprints 6, e27075v1. https://doi.org/10.7287/peerj.preprints.27075v1.
Minár, J., Evans, I.S., Jenčo, M., 2020. A comprehensive system of definitions of land surface (topographic) curvatures, with implications for their application in geoscience modelling and prediction. Earth Sci. Rev. 211, 103414 https://doi.org/10.1016/j.earscirev.2020.103414.
Mitas, L., Mitasova, H., 1998. Distributed soil erosion simulation for effective erosion prevention. Water Resour. Res. 34 (3), 505–516. https://doi.org/10.1029/97WR03347.
Mitasova, H., Hofierka, J., Zlocha, M., Iverson, L.R., 1996. Modelling topographic potential for erosion and deposition using GIS. Int. J. Geogr. Inf. Syst. 10, 629–641. https://doi.org/10.1080/02693799608902101.
Mokarram, M., Sathyamoorthy, D., 2018. A review of landform classification methods. Spat. Inf. Res. 26 (6), 647–660. https://doi.org/10.1007/s41324-018-0209-8.
Moore, I.D., Burch, G.J., Mackenzie, D.H., 1988. Topographic effects on the distribution of surface soil water and the location of ephemeral gullies. Trans. ASAE 31 (4), 1098–1107. https://doi.org/10.13031/2013.30829.
Moskalik, M., Zagórski, P., Łęczyński, L., Ćwiąkała, J., Demczuk, P., 2018. Morphological characterization of Recherchefjorden (Bellsund, Svalbard) using marine geomorphometry. Polish Polar Res. 39 (1), 99–125. https://doi.org/10.24425/118740.
Na, J., Ding, H., Zhao, W., Liu, K., Tang, G., Pfeifer, N., 2021. Object-based large-scale terrain classification combined with segmentation optimization and terrain features: a case study in China. Trans. GIS 25, 2939–2962. https://doi.org/10.1111/tgis.12795.
Najafi, S., Dragovich, D., Heckmann, T., Sadeghi, S.H., 2021. Sediment connectivity concepts and approaches. Catena 196, 104880. https://doi.org/10.1016/j.catena.2020.104880.
Neto, G.B.S., de Souza Martins, É., 2019. Semi-automatic method delimitation of basic relief units. Rev. Brasil. Geomorfol. 20 (2), 397–409 (in Portuguese).
Newman, D.R., Lindsay, J.B., Cockburn, J.M.H., 2018. Evaluating metrics of local topographic position for multiscale geomorphometric analysis. Geomorphology 312, 40–50. https://doi.org/10.1016/j.geomorph.2018.04.003.
Newman, D.R., Cockburn, J.M.H., Drăguţ, L., Lindsay, J.B., 2022. Local scale optimization of geomorphometric land surface parameters using scale-standardized Gaussian scale-space. Comput. Geosci. 165, 105144 https://doi.org/10.1016/J.CAGEO.2022.105144.
Pacina, J., 2009. Possibilities of automated georelief segmentation for the requirements of Geomorphologic information system (GmIS). Geomorphol. Slovaca Bohemica 9 (2), 37–49.
Peckham, S.D., 2011. Monkey, starfish and octopus saddles. In: Hengl, T., Evans, I.S., Wilson, J.P., Gould, M. (Eds.), Proceedings of Geomorphometry 2011. International Society for Geomorphometry, Redlands, California, pp. 31–34.
Petrikovičová, L., Rampašeková, Z., Sobocká, J., 2020. A detailed identification of erosionally endangered agricultural land in Slovakia (Case study of Nitra Upland). Sustainability 12 (12), 4863. https://doi.org/10.3390/su12124863.
Phillips, J.D., 1999. Divergence, convergence, and self-organization in landscapes. Ann. Assoc. Am. Geogr. 89, 466–488. https://doi.org/10.1111/0004-5608.00158.
Phillips, J.D., 2009. Landscape evolution space and the relative importance of geomorphic processes and controls. Geomorphology 109 (3–4), 79–85. https://doi.org/10.1016/j.geomorph.2009.01.007.
Pike, R.J., 1988. The geometric signature: Quantifying landslide-terrain types from digital elevation models. Math. Geol. 20, 491–511. https://doi.org/10.1007/BF00890333.
Pike, R.J., Acevedo, W., Card, D.H., 1989. Topographic grain automated from digital elevation models. In: Proceedings of the Ninth International Symposium on Computer Assisted Cartography, Baltimore, MD, pp. 128–137.
Piloyan, A., Konečný, M., 2017. Semi-automated classification of landform elements in Armenia based on SRTM DEM using K-means unsupervised classification. Quaest. Geograph. 36 (1), 93–103. https://doi.org/10.1515/quageo-2017-0007.
Popov, A.B., Minár, J., Gallay, M., 2021. Multiresolution land surface segmentation and generalization of DEM: tentative searching for the optimal settings of detecting

elementary forms. Trans. GIS 25 (5), 2376–2393. https://doi.org/10.1111/tgis.12842.
Queen, C.W., Nelson, F.E., Gunn, G., Nyland, K.E., 2021. A characteristic periglacial landform: Automated recognition and delineation of cryoplanation terraces in eastern Beringia. Permafr. Periglac. Process. 32 (1), 35–46. https://doi.org/10.1002/ppp.2083.
Rabanaque, M.P., Martínez-Fernández, V., Calle, M., Benito, G., 2022. Basin-wide hydromorphological analysis of ephemeral streams using machine learning algorithms. Earth Surf. Process. Landf. 47, 328–344. https://doi.org/10.1002/esp.5250.
Rennó, C.D., Nobre, A.D., Cuartas, L.A., Soares, J.V., Hodnett, M.G., Tomasella, J., Waterloo, M.J., 2008. HAND, a new terrain descriptor using SRTM-DEM: Mapping terra-firme rainforest environments in Amazonia. Remote Sens. Environ. 112, 3469–3481. https://doi.org/10.1016/j.rse.2008.03.018.
Riley, S.J., DeGloria, S.D., Elliot, R., 1999. A terrain ruggedness index that quantifies topographic heterogeneity. Int. J. Sci. 5 (1–4), 23–27.
Roering, J.J., Kirchner, J.W., Dietrich, W.E., 2001. Hillslope evolution by nonlinear, slope-dependent transport: Steady state morphology and equilibrium adjustment timescales. J. Geophys. Res. Solid Earth 106 (B8), 16499–16513. https://doi.org/10.1029/2001JB000323.
Romstad, B., Etzelmüller, B., 2012. Mean-curvature watersheds: a simple method for segmentation of a digital elevation model into terrain units. Geomorphology 139, 293–302. https://doi.org/10.1016/j.geomorph.2011.10.031.
Sărășan, A., Józsa, E., Ardelean, A.C., Drăguț, L., 2019. Sensitivity of geomorphons to mapping specific landforms from a digital elevation model: a case study of drumlins. Area 51, 257–267. https://doi.org/10.1111/area.12451.
Savigear, R.A.G., 1965. A technique of morphological mapping. Ann. Assoc. Am. Geogr. 55, 514–538. https://doi.org/10.1111/j.1467-8306.1965.tb00532.x.
Schmidt, J., Andrew, R., 2005. Multi-scale landform characterization. Area 37 (3), 341–350. https://www.jstor.org/stable/20004468.
Schmidt, J., Hewitt, A., 2004. Fuzzy land element classification from DTMs based on geometry and terrain position. Geoderma 121 (3–4), 243–256. https://doi.org/10.1016/j.geoderma.2003.10.008.
Scown, M.W., Thoms, M.C., De Jager, N.R., 2015. Floodplain complexity and surface metrics: Influences of scale and geomorphology. Geomorphology 245, 102–116. https://doi.org/10.1016/j.geomorph.2015.05.024.
Seijmonsbergen, A.C., 2013. The modern geomorphological map. In: Shroder, J., Switzer, A.D., Kennedy, D.M. (Eds.), Treatise on Geomorphology. Academic Press, San Diego, pp. 35–52.
Seijmonsbergen, A.C., Hengl, T., Anders, N.S., 2011. Semi-automated identification and extraction of geomorphological features using digital elevation data. Develop. Earth Surf. Proc. 15, 297–335. https://doi.org/10.1016/B978-0-444-53446-0.00010-0.
Shary, P.A., 1995. Land surface in gravity points classification by a complete system of curvatures. Math. Geol. 27 (3), 373–390. https://doi.org/10.1007/BF02084608.
Shary, P.A., Sharaya, L.S., Mitusov, A.V., 2002. Fundamental quantitative methods of land surface analysis. Geoderma 107 (1–2), 1–32. https://doi.org/10.1016/S0016-7061(01)00136-7.
Shary, P.A., Sharaya, L.S., Mitusov, A.V., 2005. The problem of scale-specific and scale-free approaches in geomorphometry. Geogr. Fis. Din. Quat. 28 (1), 81–101.
Shumack, S., Hesse, P., Farebrother, W., 2020. Deep learning for dune pattern mapping with the AW3D30 global surface model. Earth Surf. Process. Landf. 45 (11), 2417–2431. https://doi.org/10.1002/esp.4888.
Siervo, V., Pescatore, E., Giano, S.I., 2023. Geomorphic analysis and semi-automated landforms extraction in different natural landscapes. Environ. Earth Sci. 82, 128. https://doi.org/10.1007/s12665-023-10823-4.
Siqueira, R.G., Veloso, G.V., Fernandes-Filho, E.I., Francelino, M.R., Schaefer, C.E.G.R., Corrêa, G.R., 2022. Evaluation of machine learning algorithms to classify and map landforms in Antarctica. Earth Surf. Process. Landf. 47 (2), 367–382. https://doi.org/10.1002/esp.5253.
Sîrbu, F., Drăguț, L., Oguchi, T., Hayakawa, Y., Micu, M., 2019. Scaling land-surface variables for landslide detection. Prog. Earth Planet Sci. 6, 44. https://doi.org/10.1186/s40645-019-0290-1.
Small, E.E., Anderson, R.S., Hancock, G.S., 1999. Estimates of the rate of regolith production using ^{10}Be and ^{26}Al from an alpine hillslope. Geomorphology 27, 131–150. https://doi.org/10.1016/S0169-555X(98)00094-4.
Smerlak, M., 2021. Intermittency as metastability: a predictive approach to evolution in rugged landscapes. Earth Planet. Sci. Lett. 134 (2), 28002. https://doi.org/10.1209/0295-5075/134/28002.
Sofia, G., 2020. Combining geomorphometry, feature extraction techniques and Earth-surface processes research: the way forward. Geomorphology 355, 107055. https://doi.org/10.1016/j.geomorph.2020.107055.
Sofia, G., Bailly, J.S., Chehata, N., Tarolli, P., Levavasseur, F., 2016. Comparison of Pleiades and LiDAR digital elevation models for terraces detection in farmlands. IEEE J. Sel. Top. Appl. Earth Obs. Rem. Sens. 9 (4), 1567–1576. https://doi.org/10.1109/JSTARS.2016.2516900.
Speight, J.G., 1974. A parametric approach to landform regions. In: Brown, E.H., Waters, R.S. (Eds.), Progress in Geomorphology: Papers in Honour of David L. Linton. Institute of British Geographers Special Publication 7. Alden Press, London, pp. 213–230.
Strahler, A.N., 1952. Hypsometric (area-altitude) analysis of erosional topography. Bull. Geol. Soc. Am. 63, 1117–1141. https://doi.org/10.1130/0016-7606(1952)63[1117:HAAOET]2.0.CO;2.
Tarolli, P., Sofia, G., 2016. Human topographic signatures and derived geomorphic processes across landscapes. Geomorphology 255, 140–161.
Tarolli, P., Sofia, G., Dalla Fontana, G., 2012. Geomorphic features extraction from high-resolution topography: landslide crowns and bank erosion. Nat. Hazards 61 (1), 65–83. https://doi.org/10.1007/s11069-010-9695-2.
Trentin, R., Robaina, L.E.S., 2018. Estudo dos elementos de relevo da bacia hidrográfica do rio Ibicuí com o uso do índice de posição topográfica. Rev. Brasil. Geomorfol. 19, 423–431.
Troeh, F.R., 1964. Landform parameters correlated to soil drainage. Soil Sci. Amer. Proc. 28 (6), 808–812. https://doi.org/10.2136/sssaj1964.03615995002800060035x.
van der Meij, W.M., Meijles, E.W., Marcos, D., Harkema, T.T., Candel, J.H., Maas, G.J., 2022. Comparing geomorphological maps made manually and by deep learning. Earth Surf. Process. Landf. 47 (4), 1089–1107. https://doi.org/10.1002/esp.5305.
van Niekerk, A., 2010. A comparison of land unit delineation techniques for land evaluation in the Western Cape, South Africa. Land Use Policy 27, 937–945. https://doi.org/10.1016/j.landusepol.2009.12.007.
Vandaele, K., Poesen, J., Govers, G., van Wesemael, B., 1996. Geomorphic threshold conditions for ephemeral gully incision. Geomorphology 16 (2), 161–173. https://doi.org/10.1016/0169-555X(95)00141-Q.
Venditti, J.G., Li, T., Deal, E., Dingle, E., Church, M., 2020. Struggles with stream power: Connecting theory across scales. Geomorphology 366, 106817. https://doi.org/10.1016/j.geomorph.2019.07.004.
Walker, S.J., Wilkinson, S.N., van Dijk, A.I.J.M., Hairsine, P.B., 2020. A multi-resolution method to map and identify locations of future gully and channel incision. Geomorphology 358, 107115. https://doi.org/10.1016/j.geomorph.2020.107115.
Wei, H., Li, S., Li, C., Zhao, F., Xiong, L., Tang, G., 2021. Quantification of loess landforms from three-dimensional landscape pattern perspective by using DEMs. ISPRS Int. J. Geo Inf. 10 (10), 693. https://doi.org/10.3390/ijgi10100693.
Weiss, A.D., 2001. Topographic positions and landforms analysis (Map gallery poster). In: Proceedings of the 21st Annual ESRI User Conference. San Diego, CA.
Wieczorek, M., Migoń, P., 2014. Automatic relief classification versus expert and field-based landform classification for the medium–altitude mountain range, the Sudetes, SW Poland. Geomorphology 206, 133–146. https://doi.org/10.1016/j.geomorph.2013.10.005.
Wood, J.D., 1996. The Geomorphological Characterisation of Digital Elevation Models. PhD Thesis. University of Leicester, UK https://lra.le.ac.uk/handle/2381/34503 (accessed 11 July 2019).
Woodcock, C., Strahler, A.H., 1987. The factor of scale in remote sensing. Remote Sens. Environ. 21 (3), 311–332. https://doi.org/10.1016/0034-4257(87)90015-0.
Woodrow, K., Lindsay, J.B., Berg, A.A., 2016. Evaluating DEM conditioning techniques, elevation source data, and grid resolution for field-scale hydrological parameter extraction. J. Hydrol. 540, 1022–1029. https://doi.org/10.1016/j.jhydrol.2016.07.018.
Xie, X., Zhou, X., Xue, B., Xue, Y., Quin, K., Li, J., Yang, J., 2021. Aspect in topography to enhance fine-detailed landform element extraction on high-resolution DEM. Chin. Geogr. Sci. 31 (5), 915–930. https://doi.org/10.1007/s11769-021-1233-5.
Xiong, L.Y., Tang, G.A., Zhu, A.X., Qian, Y.Q., 2017. A peak-cluster assessment method for the identification of upland planation surfaces. Int. J. Geogr. Inf. Sci. 31 (2), 387–404. https://doi.org/10.1080/13658816.2016.1205193.
Xiong, L., Guoan, T., Yang, X., Fayuan, F., 2021. Geomorphology-oriented digital terrain analysis: progress and perspectives. J. Geogr. Sci. 31 (3), 456–476. https://doi.org/10.1007/s11442-021-1853-9.
Xiong, L., Li, S., Tang, G., Strobl, J., 2022. Geomorphometry and terrain analysis: data, methods, platforms and applications. Earth Sci. Rev. 233, 2022104191. https://doi.org/10.1016/j.earscirev.2022.104191.
Yokoyama, R., Shirasawa, M., Pike, R.J., 2002. Visualizing topography by openness: a new application of image processing to digital elevation models. Photogramm. Eng. Remote. Sens. 68, 257–265.
Zhang, W., Qi, J., Wan, P., Wang, H., Xie, D., Wang, X., Yan, G., 2016. An Easy-to-Use Airborne LiDAR Data Filtering Method based on Cloth simulation. Remote Sens. 8 (6), 501. https://doi.org/10.3390/rs8060501.
Zhou, Q., Chen, Y., 2011. Generalization of DEM for terrain analysis using a compound method. ISPRS J. Photogramm. Remote Sens. 66 (1), 38–45. https://doi.org/10.1016/j.isprsjprs.2010.08.005.